UCLouvain

AGRO LOUVAIN

Faculté des bioingénieurs

Nanomechanics of the molecular complexes between SpsD/SpsL staphylococcal adhesins and elastin

Autor: Constance Chantraine
Supervisors: Prof. Yves Dufrêne (UCLouvain/LIBST), Dr. Marion Mathelié-Guinlet (UCLouvain/LIBST)
Readers: Prof. David Alsteens (UCLouvain/LIBST), Prof. Pascal Hols (UCLouvain/LIBST)
Academic year 2019-2020
Thesis presented in partial fulfillment of the requirements for the degree of Master in Bioengineering: chemistry and bioindustries

Nanomechanics of the molecular complexes between SpsD/SpsL staphylococcal adhesins and elastin

Autor: Constance Chantraine
Supervisors: Prof. Yves Dufrêne (UCLouvain/LIBST), Dr. Marion Mathelié-Guinlet (UCLouvain/LIBST)
Readers: Prof. David Alsteens (UCLouvain/LIBST), Prof. Pascal Hols (UCLouvain/LIBST)
Academic year 2019-2020
Master in bioengineering: chemistry and bioindustries

Acknowledgments

The first person I would like to thank is my supervisor Prof. Yves Dufrêne, who gave me the opportunity to carry out my master thesis in the nBio lab. Thanks to the LBRNA2202 course, he made me discover the AFM and its diverse appealing applications. His passion for the subject transmitted during the lectures definitively reinforced me in my choice, and rightly so.

My second thank goes, of course, to my co-supervisor, Dr. Marion Mathelié-Guinlet, who trained me at AFM, teaching me, with rigor and precision, the technical aspects of the experiments and all the related theory. Her priceless mentoring was instrumental in the professional maturity gained during this master thesis. I can't be anything but infinitely grateful.

I also want to warmly thank Dr. Felipe Viela Bovio, who also took great care of every single step of my work, with patience and benevolence. Where Marion taught me how to do things right, Felipe definitively taught me perseverance and adaptation when it didn't work, forming together an outstanding team.

I am so thankful to every member of the nBio lab for all the tips and advice they gave me, but more importantly, for the convivial atmosphere they allowed me to evolve in. Among them, I would like to especially thank Simon Petitjean, for all his wise and relevant advice and also for his permanent good mood.

In addition, I am thankful to our collaborators Pietro Speziale and Giampiero Pietrocola from the Department of Molecular Medicine, Unit of Biochemistry, Pavia, Italy for providing the bacterial cultures.

I also express my gratitude to Prof. David Alsteens and Prof. Pascal Hols who accepted to read my master thesis and to be part of my jury.

I would also like to thank my family, Dad, Mom, Camille, Clément, and Filou for their unfailing support but also all my friends, especially Laura without whom Celine would not shine the same way.

Finally, this is sadly for me, also perhaps the last opportunity to thank someone special whose motivation, devotion and commitment have made these years of study such an enriching journey. Thank you Vincent, for teaching me that it is our choices that show what we truly are, far more than our abilities. I hope one day I will be worthy of the Excellence Palace.

Abstract

Staphylococcus pseudintermedius is a commensal pathogen having the capacity to develop biofilms. Bacterial adhesion to the host extracellular matrix (mainly dogs but humans too) is known to be mediated by the SpsD and SpsL adhesins. Considering the emergence of zoonosis cases for *S. pseudintermedius* and the increasing occurrence of methicillin-resistant strains, it is now crucial to unravel the mechanisms by which the pathogen adheres to-, and in turn infect, its hosts. In this context, we studied the strength and dynamics of interaction between SpsD/SpsL and elastin, a key matrix protein critical to the elasticity and resilience of many vertebrate tissues. To this end, we used atomic force microscopy, which allows to quantify the mechanical strength of single receptor-ligand complexes. We observed a bimodal distribution of the forces and rupture lengths with an inverse correlation between both parameters. These so called low and high force regimes suggest two different binding mechanisms. We also found that both SpsD- and SpsL-elastin interactions are mechanically activated. Weak binding dominates at low stress, whereas strong binding is favored at high stress. We suggest that the ultrastrong Sps-elastin interaction could result from a variation of the "dock, lock and latch" mechanism whereas the low adhesion force results from a weaker binding mechanism. Our results offer promise for the design of novel anti-adhesion strategies thereby helping in the prevention of biofilm formation and infection.

List of figures

List of tables

List of abbreviations

A (Ala)	alanine
aa	amino acids
AFM	atomic force microscopy
BHI	brain heart infusion
CWA	cell wall anchored
DFS	dynamic force spectrum
DLL	dock, lock and latch
EBP	elastin binding protein
EbpS	*S. aureus* elastin binding protein
ECM	extracellular matrix
EDC	1-ethyl-3-(3- dimethylaminopropyl)- carbodiimide
ELISA	enzyme-linked immunosorbent assay
EPM	extracellular polymer matrix
EPS	extracellular polymer substance
FD curve	force-distance curve
Fg	fibrinogen
Fn	fibronectin
FnBPs	*S. aureus* fibronectin binding protein
FV	force volume
G (Gly)	glycine
IgG	immunoglobulin G
K_D	dissociation constant
kDa	kilodaltons
K_m	spring constant of the molecular complex
K (Lys)	lysine
LOX	lysyl oxidase
LR	loading rate
MRSP	methicillin-resistant *S. pseudintermedius*
MSCRAMMs	microbial surface components recognizing adhesive matrix molecules
MSSP	methicillin- sensitive *S. pseudintermedius*
NHS	N-hydroxysuccinimide
P (Pro)	proline
PBS	phosphate buffer saline
QI	quantitative imaging
RER	rough endoplasmic reticulum
s.d.	standard deviation
SAMs	self-assembled monolayers
SCFS	single cell force spectroscopy
SMFS	single molecule force spectroscopy
Sps	*S. pseudintermedius* surface protein
STM	scanning tunnel microscope
TEM	transmission electron microscopy
TBS	tris Buffer Saline
V (Val)	valine

Table of contents

1. Origin of staphylococci pathogenicity

The first chapter will introduce the main concepts used in this thesis, starting with (i) a general perspective on one of the ubiquitous bacterial lifestyle leading to increased pathogenicity, the biofilms (1.1), focusing then on (ii) a staphylococcal species affecting both humans and animals, *Staphylococcus pseudintermedius* (*S. pseudintermedius,* 1.2). The scope of this thesis will finally be addressed when describing the virulence factors such bacteria develop (1.3) to interact with their host, notably proteins of the extracellular matrix (1.4).

1.1 Biofilm, a bacterial lifestyle to resist external stresses

1.1.1 Definition and implication

A biofilm is a structured consortium of bacteria (from a single or multiple microbial species), with a high cell density ranging from 10^8 to 10^{11} cells/g of wet weight, adhered to a substratum and embedded in a self-produced extracellular polymer substance (EPS) also called extracellular polymer matrix (EPM) (Figure 1) (Pompilio *et al.*, 2015) (Flemming *et al.*, 2016) (Flemming and Wingender, 2010). These extracellular polymers include various types of polysaccharides, a range of different proteins, extracellular nucleic acids, amphiphilic compounds, and extracellular membrane vesicles as well as bacterial refractory compounds (Neu and Lawrence, 2015). This EPM provides its inhabitant cells with (i) protection from chemical or physical injuries, by providing a water, enzyme and nutrient retention and (ii) anchors and stabilizes the biofilm.

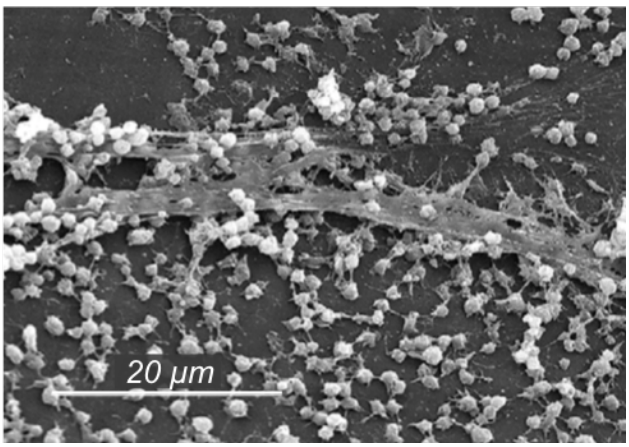

Figure 1: Scanning electron micrograph of a staphylococcal biofilm on the inner surface of an indwelling medical device (Donlan, 2002).

Biofilms are one of the most widely distributed and successful modes of life for microbes on Earth (Kolter and Greenberg, 2006), and they drive processes such as biogeochemical cycling of most elements in water, soil, sediment and subsurface environments. At first sight, biofilms can be beneficial to some biotechnological applications, including for example the degradation

of wastewater/solid waste and biocatalysis in biotechnological processes, such as the production of bulk and fine chemicals, as well as biofuels (Halan *et al.*, 2012). Concerning the human health, even if most studies have focused on biofilms associated with diseases, they can also have a positive impact on the function of the intestinal microbiota for example, facilitating the digestion of polysaccharides (Macfarlane and Dillon, 2007),(de Vos, 2015).

1.1.2 Steps in biofilm formation

Biofilm formation occurs in few common steps: initial contact/attachment to the surface, micro-colony formation, maturation and formation of the architecture of the biofilm, and finally detachment/dispersion of the biofilm (Figure 2).

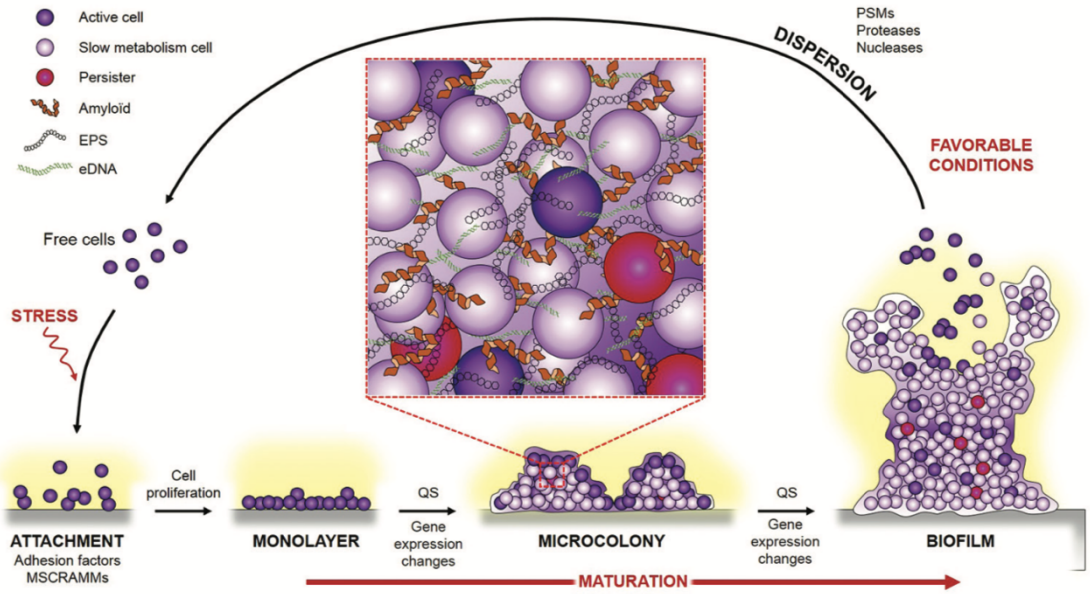

Figure 2: Scheme of the biofilm formation process (Reffuveille et al., 2017).

- Initial contact/attachment to the surface

During the first step of biofilm formation, bacteria go from the planktonic to the attached form. The microbial cells are attracted to the surface via physical forces like van der Waal's forces and electrostatic interactions. At some point, close to the surface, those physical forces can be repulsive, so they use non-specific factors, such as pili and fimbriae, but also specific factors called adhesins, which regulate specific adhesion, to attach to the surface. This adhesion precedes the cohesion which is the interaction/attachment in between cells. The interaction is still reversible when only physical forces are involved and become irreversible when bacteria establish physical contact with surface through adhesins or pili (Garrett *et al.*, 2008).

- Micro-colony formation

Once the attachment becomes stable, a process of multiplication of microbial cells starts, initiated through particular chemical signaling within the EPS. This process leads to the formation of micro-colonies. During this step, the transcription of genes coding for the synthesis of structures such as flagella is stopped since the bacteria do not need to be motile anymore. Conversely, the genes coding for structures such as adhesins are overexpress allowing a better adhesion.

- Maturation and architecture

Then, bacteria further develop the EPS which provides strength to the interaction of microorganisms within the biofilm. Typically, the microorganism represents 5 to 35% of the biofilm volume while the remaining volume is constituted of EPS. Thanks to this structure some important nutrients and minerals are trapped from the surrounding environment through this scavenging system.

- Detachment/dispersion of biofilm

In response to environmental changes such as nutrient starvation, shear stress or other mechanical forces, microbial cells within the biofilm perform quick multiplication and dispersion in order to convert from sessile into motile form. Fragments of biofilm or isolated bacteria are then released to form a new biofilm in another area of the substrate (Lebeaux and Ghigo, 2012). In this phase microbial cells upregulate the expression of proteins related to bacterial motility, to let the bacteria migrate to a new site. Detachment of microbial cells and transfer to a new site aid in the spreading of infections (Jamal *et al.*, 2018).

1.1.3 Infections associated with biofilm

Though eventually helpful for some biotechnological processes and/or for the well establishment of the human microbiota, biofilms can also and would provoke some persistent infections under specific conditions (Costerton *et al.*, 1999). Indeed, all higher organisms, including humans, are colonized by microorganisms that form biofilms. Those biofilms can be associated with persistent infections in organisms and with the contamination of medical devices and implants. Moreover, bacterial biofilms are of clinical relevance since they confer resistance to antibiotics and disinfectants, as well as resistance to phagocytosis and to the host immune system in general, (Pompilio *et al.*, 2015). Biofilms show indeed an ability to resist to antibiotics leading to recalcitrance of infectious diseases. While the bulk of cells in the biofilm are actually highly susceptible to killing by antibiotics, a small fraction of persistent cells remains alive. The immune system eliminates both regular cells and persisters from the bloodstream but it can not reach the inside of the biofilm. The only remaining live cells then are persistent

ones in the biofilm. Once the level of antibiotic drops, persistent cells repopulate the biofilm, and the infection relapses (Lewis, 2012).

It is estimated that about 65% of all bacterial infections are associated with bacterial biofilms (Jamal *et al.*, 2018) including *Pseudomonas aeruginosa* in cystic fibrosis pneumonia, *Haemophilus influenzae* and *Streptococcus pneumoniae* in chronic otitis media, *Staphylococcus aureus* in chronic rhinosinusitis and enteropathogenic *Escherichia coli* in recurrent urinary tract infections (Hall-Stoodley and Stoodley, 2009). These can include device- and non-device-associated infections (O'Neill *et al.*, 2008) such as dental caries, periodontitis, otitis media, musculoskeletal infections and necrotizing fasciitis (Figure 3) (Costerton *et al.*, 1999). In most of the cases, the production of biofilm favors the chronicity infections, notably due to its resistance to antibiotics and many other molecules or environmental stresses, as mentioned above. It seems that the natural resistance of biofilms comes from the induction of specific biofilm mechanisms such as the changes of many gene expressions which increase the antimicrobial resistance (Reffuveille *et al.*, 2017).

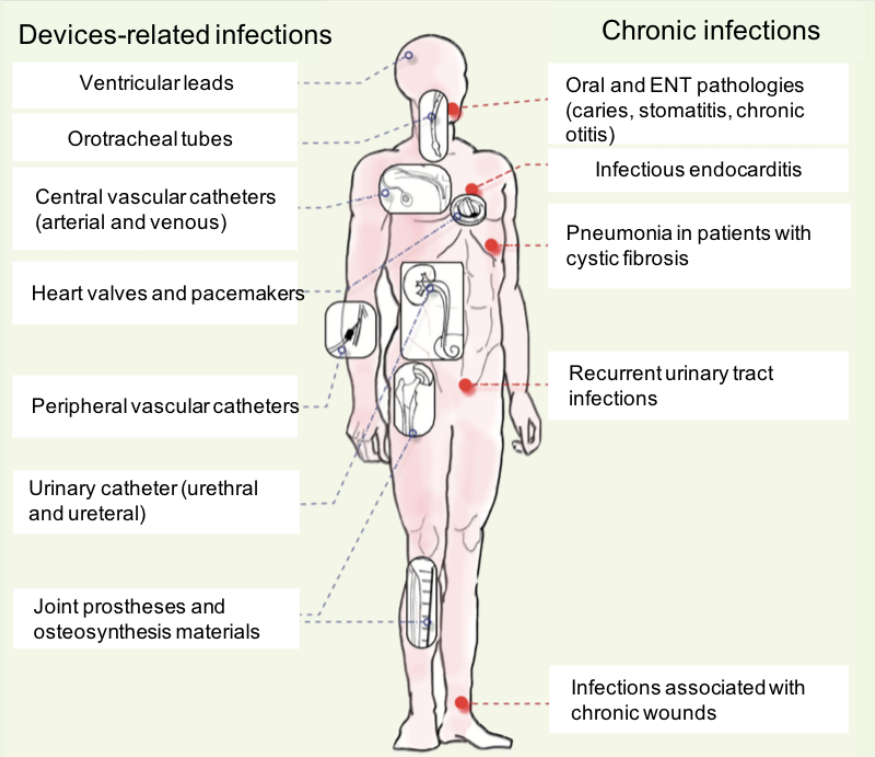

Figure 3: Main infections associated with biofilms. ENT: Ear, Nose and Throat (otorhinolaryngology) (Lebeaux and Ghigo, 2012).

In addition, the infection mechanism of pathogenic bacteria is based on the use of virulence factors which are all the microbial elements that will participate in the expression of the pathogenic power of the bacterium. These factors promote colonization of the host, bacterial multiplication and allow the bacteria to escape the host's immune system or directly cause tissue damage. Virulence factors can be subdivided into different groups: (i) adhesins or soluble factors that mediate the attachment to host cells or extracellular matrix proteins, (ii)

exoenzymes that are involved in the destruction of host tissues, (iii) toxins that directly exert detrimental effects to the host and (iv) a heterogeneous group comprising iron uptake systems, immune system evasion mechanisms, and other factors that enhance the fitness to survive in the host (Rosenstein and Gotz, 2013). The formation of biofilms is one strategy among others that helps cells to further express such factors and to resist unfavorable conditions in the host as exerted by shearing forces of the bloodstream, the immune response of the host, or anti-infective measures during disease treatment, leading to persistent infections.

Among all those bacteria, *Staphylococcus* is the leading genius in this domain of infections associated with biofilm (especially *Staphylococcus aureus*) (Reffuveille *et al.*, 2017). Biofilm formation is now recognized as one of the most important aspects in several *Staphylococcus spp* virulence (Singh et al 2013) (Pompilio *et al.*, 2015). The colonization of implanted materials by staphylococcal biofilm is one of the highest important issues. Staphylococcal biofilm can develop on various structures such as catheters, prosthetic joints, prosthetic heart valves, contact lenses, cerebrospinal fluid shunts and cardiac pacemakers (Figure 3). Dramatically, after their implantation in the body, medical devices become coated with host proteins, facilitating the attachment of bacteria and the biofilm formation. Consequently, staphylococcal biofilm formation is linked to various diseases such as endocarditis, osteomyelitis, skin and soft tissues infections, urinary tract infection, nasal colonization and cystic fibrosis complications as well as implant-associated infections (Lebeaux *et al.*, 2013).

1.2 *Staphylococcus pseudintermedius*, an opportunistic pathogen

1.2.1 Commensal *S. pseudintermedius*

In the large family of staphylococci, *Staphylococcus pseudintermedius,* a potential pathogen for domestic animals presents similar infection mechanisms and effects as *Staphylococcus aureus* for humans. Immobile and not spore-forming, this microorganism is about 0,5 to 1,5 µm in diameter, grows easily on usual culture media and form round, white and smooth colonies up to 4 mm in diameter. Like other Gram-positive bacteria, it has a wall composed of peptidoglycans, teichoic acids and proteins (Figure 4 left). Due to its commensal nature, *S. pseudintermedius* will only cause damage if the host's defense mechanisms (*e.g.* skin barrier) are altered making it an opportunistic pathogen. Various predisposing factors and primary causes of infection contribute to the switch of *S. pseudintermedius* from commensal to pathogen (Bajwa, 2016). It is recognized as the leading cause of skin, ear, and post-operative bacterial infections in dogs (Pompilio *et al.*, 2015) (Bajwa, 2016).

In healthy dogs, *S. pseudintermedius* is part of the normal cutaneous microflora and colonizes the skin, hair follicles/coat and, in particular, mucocutaneous sites, such as the nose, mouth and anus following different rates (Figure 4 right). It constitutes about 90% of staphylococci

isolated from canine healthy carriers (Bannoehr and Guardabassi, 2012). It has been previously shown that most dogs are either persistent or intermittent carriers, and very few individuals are non-carriers (Paul *et al.*, 2013). Since it resides as part of the normal flora of most dogs it will not cause any disease in normal conditions.

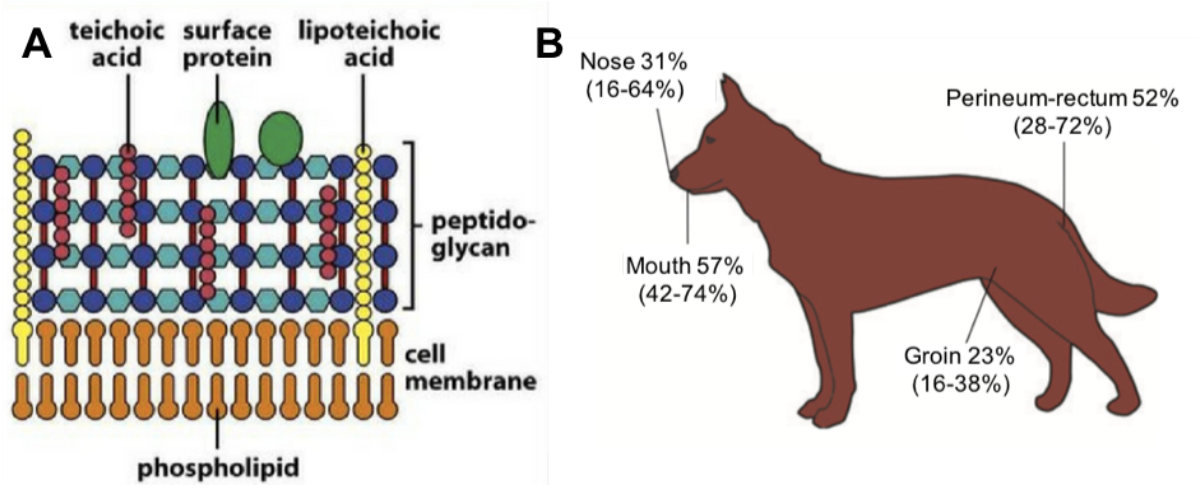

Figure 4: Schematic representation of gram positive cell wall (left) and Staphylococcus pseudintermedius carriage rates per body sites in dogs (% of carrier dogs) (right) (Bannoehr and Guardabassi, 2012).

1.2.2 Pathogenecity of *S. pseudintermedius*

In infected dogs, when the resistance of the host is lowered, and the skin barrier altered by predisposing factors, such as atopic dermatitis, medical and surgical procedures, *S. pseudintermedius* is able to induce disease such as pyoderma (Bannoehr and Guardabassi, 2012). This is one of the most common diseases seen in small-animal veterinary practice worldwide (Bannoehr *et al.*, 2011) and caused predominantly by this pathogen (Bajwa, 2016). It consists in an infection of the different skin layers, causing erythema, crusts, pustules, ulcers or even going as far as necrosis (Hnilica and Patterson, 2017). Moreover, this staphylococcal species can also be involved in ear infections (such as otitis externa which is an inflammation of the ear canal) and in nearly any type of community- and hospital-acquired infections (Bannoehr and Guardabassi, 2012). This bacterium represents 90% of staphylococci isolated from sick dogs making it the most frequent bacterial pathogen isolated from clinical canine specimens (Bannoehr and Guardabassi, 2012).

Even if dogs are the principal host, humans can also be affected by *S. pseudintermedius* (Wladyka *et al.*, 2015). Numerous examples showing the transmission of a *S. pseudintermedius* from a dog to its owner can be found in literature (van Duijkeren, 2011). The first case of zoonosis induced by this bacterium was discovered and reported by Van Hoovels *et al.* in 2006, (Van Hoovels *et al.*, 2006). Since then, cases multiplied. This species recognized primarily as an important canine pathogen is increasingly being identified in human infections (Little *et al.*, 2019).

Recently, *Staphylococcus pseudintermedius* has been found to have the potential to grow as a biofilm in dogs (its natural host) but also in human (Singh *et al.*, 2013) (Pompilio *et al.*, 2015). A study lead in 2013 by Singh *et al.* demonstrated that 97% of *S. pseudintermedius* isolates tested were able to produce moderately to strongly *in vitro* biofilm. The presence of aggregates of cocci in addition to large amounts of irregularly produced EPS on stainless steel was observed using scanning electron microscopy (Figure 5). They also found out that there was no difference in ability to form biofilm between methicillin-resistant *S. pseudintermedius* (MRSP) and methicillin-sensitive *S. pseudintermedius* (MSSP), (Singh *et al.*, 2013). Those results were confirmed by Casagrande Proietti *et al.* in 2015 who found that a majority of *S. pseudintermedius* isolates tested (96%) were able to produce biofilms *in vitro*, using three other phenotypic characterization methods (Casagrande Proietti *et al.*, 2015). In cases of *S. pseudintermedius* biofilms, the treatment of such pathogens is made even more complicated given the protection offered by this structure (Jørgensen *et al.*, 2016).

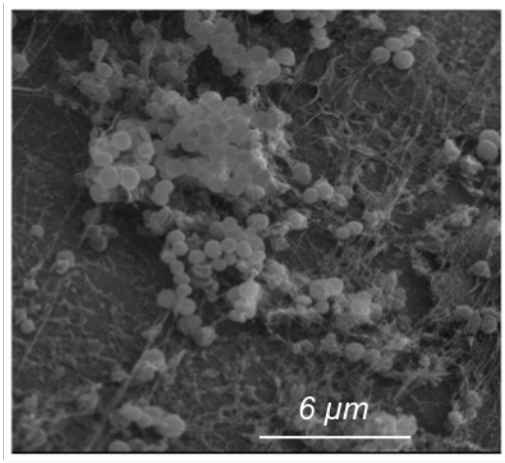

Figure 5: SEM Images of MRSP biofilm formation on 316L stainless steel orthopedic bone screws. Large aggregates of cocci and irregularly produced extracellular polymeric substance are apparent (Singh et al., 2013).

Over the last decade, multidrug-resistant strains have emerged worldwide especially clones that have acquired the Staphylococcal Chromosomal Cassette (SCCmec) mobilizing the methicillin resistance gene mecA. In the case of biofilm formation, the physical proximity of bacteria favors the horizontal transfer of genetic material by conjugation or transformation allowing the acquisition of genes of resistance to biocides or other beneficial characters increasing the chances of survival of the community (Lebeaux and Ghigo, 2012). Infections caused by MRSP can be difficult or even impossible to treat using conventional veterinary antimicrobial agents (Perreten *et al.*, 2010) (Pires dos Santos *et al.*, 2016). It has also been proved that *S. pseudintermedius* taken from human infections has the potential to grow as an antibiotic-resistant biofilm (Pompilio *et al.*, 2015). These multiresistant strains, acting as nosocomial agents in veterinary hospitals, constitute a major therapeutic and health issue (Chambeaud, 2012) and a serious challenge for veterinary dermatologists (Pompilio *et al.*, 2015).

The study of this bacterium therefore presents a double interest given that we now have to fight more and more against the zoonosis that it causes but also to face the cases of methicillin-resistance that the MRSP generate. The conventional treatments presenting low or no effect against the MRSP strains, it seems now necessary to turn to alternative strategies. In this perspective, our work relates to the study of the initial biofilm formation step, *i.e.* bacterial adhesion to the various constituent elements of the host's extracellular matrix. Unravelling the adhesion mechanisms of *S. pseudintermedius* could help in the design of novel anti-adhesion strategies thereby preventing biofilm formation and thus perturbing the infection.

1.2.3 Virulence factors of *S. pseudintermedius*

During the different steps of the infection pathway, bacteria produce various virulence factors, as mentioned above. Similarly to *S. aureus*, veterinary strains of *S. pseudintermedius* are able to produce a variety of them, as detailed in Figure 6.

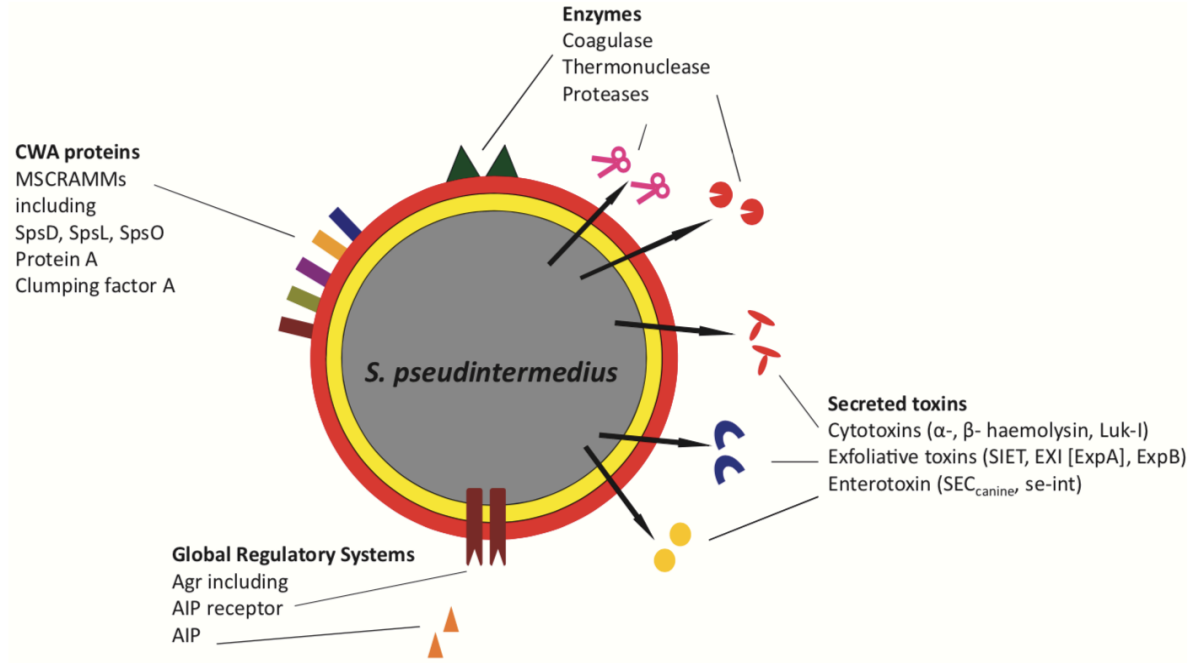

Figure 6: Simplified schematic diagram of selected cell-wall-associated and secreted virulence factors of Staphylococcus pseudintermedius. Abbreviations: Agr, accessory gene regulator; AIP, autoinducing peptide; CWA, cell-wall-anchored; EXI, exfoliative toxin of S. pseudintermedius; ExpA and ExpB, exfoliative toxin of S. pseudintermedius A and B; Luk-I, bicomponent leukotoxin; MSCRAMMs, microbial surface components recognizing adhesive matrix molecules; SIET, S. pseudintermedius exfoliative toxin; SECcanine, canine type C enterotoxin; se-int, S. intermedius enterotoxin; and Sps, S. pseudintermedius surface proteins (Bannoehr et Guardabassi, 2012).

These virulence factors have three major aims (Garbacz *et al.*, 2013). First, they enable the microorganism to spread within the host body (enzymes such as coagulases, DNases, lipases, thermonucleases and proteases): bacteria multiply on the surface of the skin by assimilating nutrients thanks to their numerous enzymes (lipases, proteases, nucleases). Secondly, these

factors modulate the host immune system (cytotoxins such as β-hemolysin, exfoliative toxins, leukotoxins, enterotoxins and protein A). For instance, toxins can cause various syndromes at a distance from the infectious site by disrupting membranes fluidity and organization or by protecting the secreted bacteria from phagocytosis. Finally, the virulence factors enable adhesion to host cells or extracellular matrix (ECM) (surface proteins such as clumping factor and adhesins). This adhesion process is governed by the interactions between the surface proteins of the bacteria and the host ligands. *S. pseudintermedius* is for instance capable of adhering to the corneocytes of dogs, just like *S. aureus* adhere to human corneocytes (Chambeaud, 2012).

Following the alteration of the skin barrier, *S. pseudintermedius* will adhere better to the epidermis, corneocytes or proteins of the ECM which are exposed. This adhesion, required for skin colonization, is mediated among other by proteins called adhesins, which can bind to host ligands like fibronectin (Fn), fibrinogen (Fg), elastin of the ECM or cytokeratin 10 of keratinocytes (Pietrocola et al, 2013). Structures such as teichoic acids from the bacterial wall and clumping factor A could also have similar role as the adhesins. Bacteria can then multiply on the surface of the skin by assimilating nutrients, develop biofilm and become pathogenic (Chambeaud, 2012).

1.3 SpsD and SpsL, key adhesins for *S. pseudintermedius* virulence

1.3.1 Cell wall anchored (CWA) adhesins

Among all the stages constituting the infectious mechanism, one of the most crucial step required for bacterial colonization and infection is the specific attachment of microorganisms to the host cells (Bannoehr and Guardabassi, 2012), (Paul *et al.*, 2013). At the molecular level, the specific adhesion of staphylococci, not only *S. pseudintermedius*, is notably mediated by some specific proteins binding to the ECM called adhesins. Each species of *staphylococcus* has its own group of adhesins, which contributes to the host specificity presented by these bacteria (Chambeaud, 2012). Thus, Bannoehr *et al.* predicted in 2011 by bioinformatic analysis, 18 genes in the genome of *S. pseudintermedius* coding for surface proteins which they named SpsA to SpsR (for *Staphylococcus pseudintermedius* surface protein) and which could have the role of adhesins (Figure 7) (Bannoehr *et al.*, 2011).

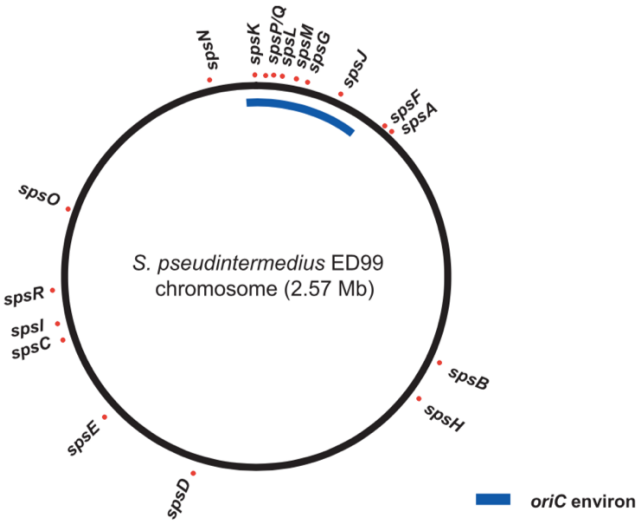

Figure 7: Genome location and distribution of genes encoding CWA proteins in S. pseudintermedius. Genome map of S. pseudintermedius ED99 indicating the genomic location of each gene (Bannoehr et al., 2011).

Because of their specific structure, these Sps are similar to the microbial surface components recognizing adhesive matrix molecules (MSCRAMMs) commonly found in staphylococci. These proteins with a predicted minimum length of approximately 250 amino acids (aa) contain one or more sequence motifs typical of CWA proteins. These motifs include an N-terminal signal sequence, characteristic repeat regions, an A domain with IgG-like folds and a C-terminal sorting signal including a LPXTG cell wall anchor motif (Figure 8).

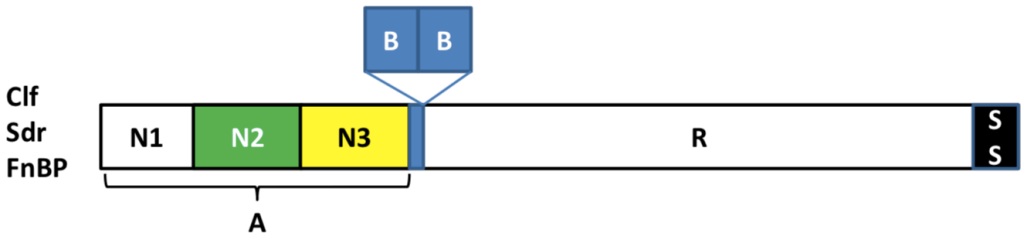

Figure 8: Domain Organization of Microbial Surface Components Recognizing Adhesive Matrix Molecules (MSCRAMMs). The archetypal MSCRAMM families Clf-Sdr-FnBP have A domains at their N termini with N2-N3 or N1-N2 comprising the minimum ligand-binding subdomains. The Sdr proteins have two to five B repeats located between the A domain and the extended unfolded repeat region R. MSCRAMM proteins have an N terminal secretory signal sequence (not shown) and a C terminal sorting signal (SS) for anchorage to peptidoglycan (Foster, 2019).

Among the 18 predicted adhesins, 9 of them are homologous with *S. aureus* adhesins. Two of them show high level of identity with *S. aureus* Fn binding proteins (FnBPs), surface proteins D and L, namely SpsD (36% of identity) and SpsL (27% of identity), which are recognized as an important virulence factor for *S. pseudintermedius* (Bannoehr *et al.*, 2011) (Chambeaud, 2012). Expression of these protein during infection of dogs are confirmed by the identification of immunoglobulin G (IgG) specific for SpsD and SpsL in sera from dogs with bacterial pyoderma (Bannoehr *et al.*, 2011). It is for all these reasons that we have carried out our research on these two adhesins which are the ones presenting the most important role in the adhesion process.

1.3.2 *S. pseudintermedius* surface protein D and L

The structure of both SpsD and SpsL have been described, along with their potential interactions with proteins of the ECM by Pietrocola *et al.* (Pietrocola *et al.*, 2013). On one hand, the primary translation product of the SpsD gene contains 1,031 residues, has an N-terminal secretory signal sequence and a C-terminal cell wall-anchoring domain as previously described. The N-terminal end of SpsD consists of an A domain predicted to fold into three independent subdomains N1 N2 and N3 (Pietrocola *et al.*, 2013). This domain is followed by a connecting region, region C and the repeat region R (Figure 9A). The A domain is 40 % identical to the fibronectin binding domain of FnbpB from *S. aureus* and binds to the γ-chain of Fg, cytokeratin-10, and elastin where the minimal region required for binding is the N2N3 subdomain while the region C interacts with Fn (Pietrocola *et al.*, 2013). On the other hand, SpsL is a protein of 930 residues that includes a signal sequence at the N-terminal followed by a Fg binding A domain with two IgG-like folds (N2 and N3), a R domain containing seven tandem repeats that confer Fn-binding capacity, and a C-terminal sorting signal (Figure 9B) (Pietrocola *et al.*, 2013).

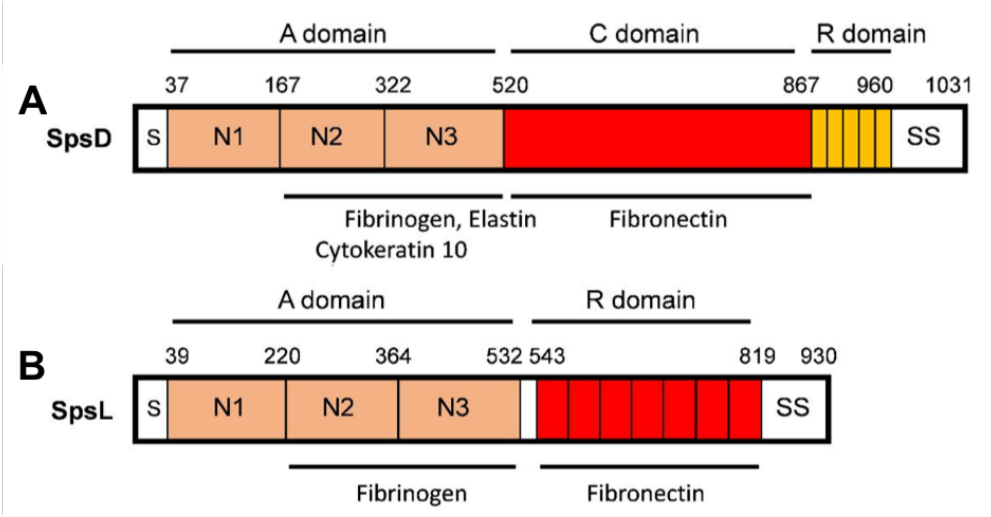

Figure 9: Schematic representation of (A) SpsD and (B) SpsL proteins from S. pseudintermedius ED99. The A domain of SpsD spans residues 37 to 519 following the signal sequence (S). This is followed by a connecting region C (residues 520-866) and a repeat region R. The number of repeats varies from strain to strain resulting in proteins of slightly different sizes. A sorting signal (SS) containing a LPXTG motif, a hydrophobic domain and a positively charged stretch occurs at the extreme C-terminus. SpsL includes a signal sequence (S) at the N-terminus, followed by an A domain (aa 39-531), a R domain containing seven tandem repeats (aa 543-818) and a C- terminal sorting signal (SS).

SpsD and SpsL promote adhesion of *S. pseudintermedius* to (i) components of the ECM proteins, such as Fn, Fg and elastin (for more details see section 1.4) and (ii) desquamated skin epithelial cells (corneocytes) of the host (Pietrocola *et al.*, 2013). SpsD and SpsL not only interact with the target molecules in the host in order to promote adhesion but also neutralize and even disrupt the biological function of their target. In addition, with its adhesion role, the SpsD A domain interferes with fibrin clot formation and platelet aggregation disrupting the coagulation process of the host (Pietrocola *et al.*, 2013). It has also been shown that both adhesins led to the development of focal skin abscesses, and while SpsD is dispensable, SpsL is required for the

development of classic *S. pseudintermedius* skin abscesses in the murine model. Richards *et al.* postulated, in 2018, that SpsL promotes abscess formation through the development of a Fg or Fn shield on the bacterial surface that could initiate bacterial aggregation (Richards *et al.,* 2018).

1.4 The ECM proteins, a preferential target for pathogens

1.4.1 The extracellular matrix

Cells in multicellular organisms are surrounded by a complex three-dimensional protein network known as the ECM which is an intricate network composed of an array of multidomain proteins. The ECM proteins can be classified into four general categories: collagens, structural glycoproteins, proteoglycans, and elastins (Tsang *et al.*, 2010). Components of the ECM link together to form a structurally stable scaffold via a network of protein/protein and protein/proteoglycan interactions, contributing to the mechanical properties of tissues. These interactions are involved in the formation of supramolecular assemblies such as collagen fibrils and elastic fibers, in tissue architecture, and in cell/matrix interactions that regulate cell growth and behavior (Yue, 2014). The ECM is also a reservoir of growth factors and bioactive molecules. It is a highly dynamic entity that is of vital importance, determining and controlling the most fundamental cellular functions (Yue, 2014). One of the most important properties of ECM is its functional diversity (Parks *et al.*, 1993). Some components are designed to be rigid, others elastic; some wet, others sticky. All have modular designs that impart diverse roles, yet allow for highly specialized functions (Mecham, 2001).

ECM proteins are privileged targets for the bacterial adhesion process (Westerlund and Korhonen,1993). In the case of *S. pseudintermedius,* Pietrocola *et al.* showed that SpsD and SpsL adhere to Fn, Fg, and α-elastin (Pietrocola *et al*., 2013), (Pietrocola *et al*., 2015). Using Surface Plasmon Resonance and ELISA-type solid-phase binding assay, they reported dissociation constants (K_D) for SpsL and SpsD towards some ECM ligands, as presented in Table 1.

Table 1: Dissociation constants (K_D) for SpsL and SpsD towards some ECM ligands. ND: not determined

	SpsD	SpsL
Fibrinogen (Fg)	0.380 μM	ND
Cytokeratin 10 (K10)	0.906 μM	ND
α-elastin	1.200 μM	ND
Fibronectin (Fn)	2.350 μM	0.81 μM

Though interactions of SpsD and SpsL with these ligands are demonstrated, the underlying molecular mechanisms from which they originate are yet to be understood and investigated.

In this context, this master thesis started focusing on the interaction between these two adhesins and a fundamental protein of the ECM, the elastin.

1.4.2 Elastin

- Overview

Elastin is a key extracellular matrix protein that is critical to the elasticity and resilience of many vertebrate tissues including large arteries, lung, ligament, tendon, skin, and elastic cartilage (Daamen *et al.*, 2006). It can contribute up to 50% of the ECM dry weight (Patel *et al.*, 2006). It is the predominant protein component of the elastic fiber that is of particular importance to the structural integrity and function of tissues in which reversible extensibility or deformability are crucial (Mecham, 2001). It is secreted as a 60-70 kilodaltons (kDa) tropoelastin monomer (Yue, 2014). This monomeric form of elastin is a soluble protein that undergoes cross-linking and assembling into elastic fibers in the extracellular matrix (Baldock *et al.*, 2011).

- Structure

Elastin consists in the cross-linking assembly of tropoelastin monomers, molecular nanosprings of about 20 nm long, that coacervate to form large elastin fibers. The process in which tropoelastin assembles into elastic fibers is classically characterized by distinct stages of tropoelastin synthesis, coacervation, microfibrillar deposition and cross-linking (Figure 10) (Yeo *et al.*, 2011).

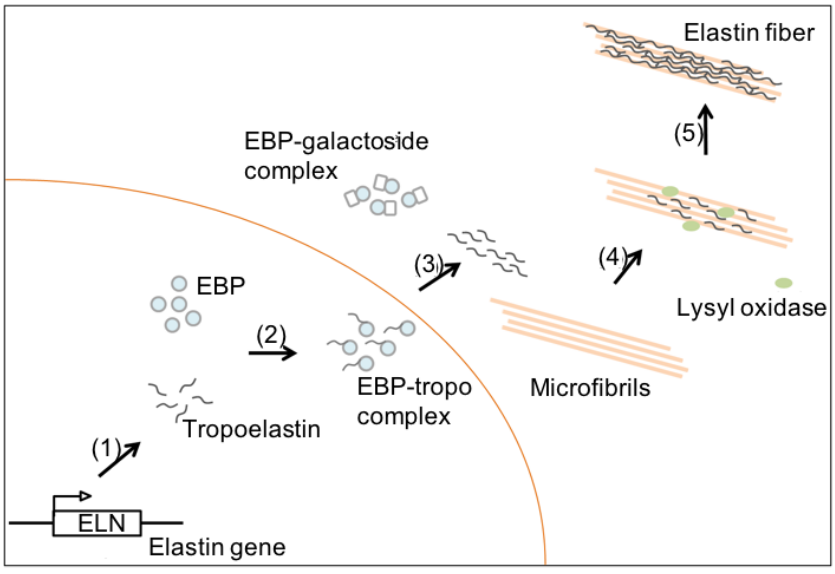

Figure 10: Schematic of the elastogenesis stages. (1) Tropoelastin is transcribed and translated from the elastin (ELN) gene and (2) transported to the plasma membrane in association with EBP. (3) Tropoelastin is released and aggregates on the cell surface, while EBP disassociates to form a complex with available galactosides. (4) Tropoelastin aggregates are oxidized by lysyl oxidase leading to crosslinked elastin that accumulates on microfibrils which help to direct elastin deposition. (5) The process of deposition and cross-linking continues to give rise to mature elastic fibers (Almine et al., 2010).

Each tropoelastin consists of a string of 36 small domains, each weighing about 2 kDa in a random coil conformation, which can extend up to 160 nm and acts as a perfect spring (Baldock *et al.*, 2011). Two major types of domains are found in tropoelastin (Figure 11A). The first ones are hydrophobic domains rich in non-polar aa especially glycine (Gly, G), valine (Val, V), proline (Pro, P) and alanine (Ala, A), and often occurring in repeats of three to six peptides such as GVGVP, GGVP and GVGVAP. The second are hydrophilic domains typically rich in lysine (Lys, K) and alanine involved in cross-linking. These domains often consist of stretches of Lys separated by two or three Ala residues such as AAAKAAKAA (Vrhovski and Weiss., 1998). Tropoelastin is synthesized in the cell (on the surface of the rough endoplasmic reticulum (RER)) and secreted to the plasma membrane via secretory vesicles. To limit its intracellular self-aggregation and its premature degradation by proteases, tropoelastin is associated with Elastin binding protein (EBP) to extracellular space (Hinek and Rabinovitch 1994).

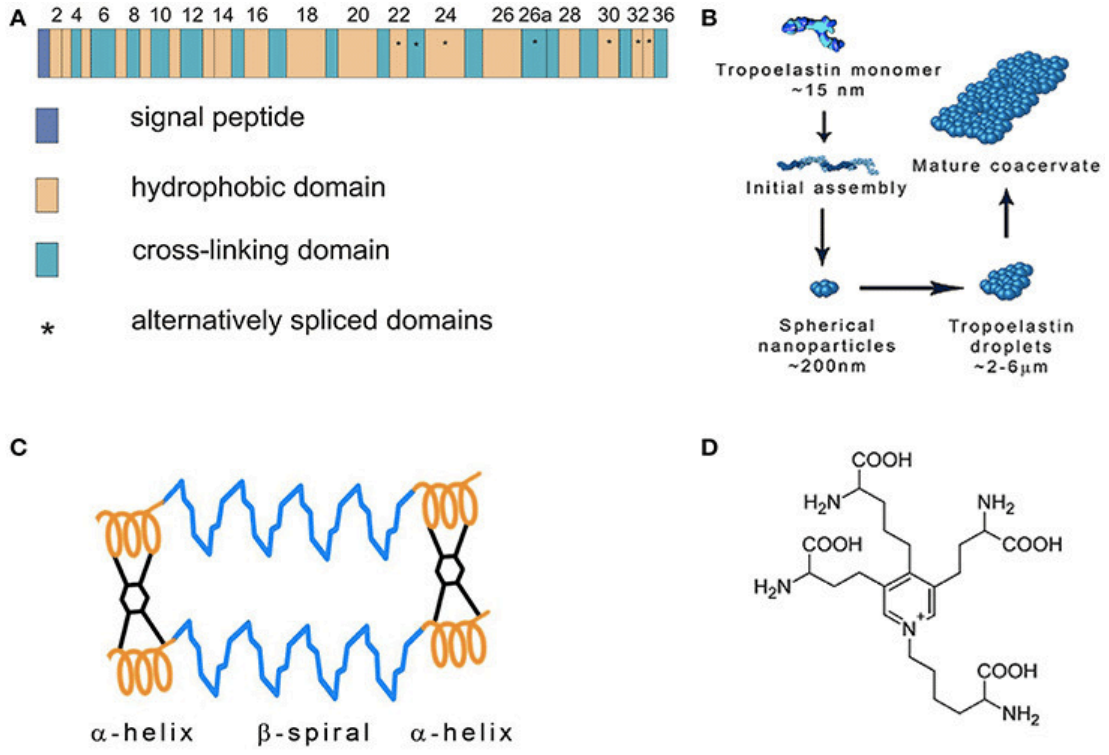

Figure 11: Overview of the Elastin feature. (A) Tropoelastin gene structure. (B) Tropoelastin (TE) assembly. TE molecules polymerize in a head-to-tail mode and subsequently coacervate. (C) Fibrillar model of elastin. Tropoelastin chains are connected with desmosine cross-links. (D) Desmosine molecule (Kanta, 2016).

In the extracellular space, tropoelastin aggregates at physiological temperature due to interactions between hydrophobic domains in a process called coacervation which represents the first major stage of elastic fiber assembly (Figure 11B). This process is reversible, thermodynamically controlled and does not require protein cleavage.

Before any elastin is deposited, microfibrils are secreted into the extracellular space close to the cell surface, marking the first step in elastogenesis. The relative elastin content increases

as elastin is laid down in small clumps which gradually fuse to form amorphous fibers. After coacervation and deposit on microfibrils, tropoelastin is rapidly rendered insoluble by cross-linking (Figure 11C). It is mediated by lysyl oxidase (LOX), which oxidizes selective lysine residues (oxidative deamination) to produce compounds that can further condense with each other to form desmosine or isodesmosine (Figure 11D) (Yue, 2014).

- Interaction with adhesins

Several pathogens, such as *Mycobacterium tuberculosis* and *Leptospira spp*., have been demonstrated to bind elastin and tropoelastin (Kuo *et al.*, 2013), (Lin *et al.*, 2009). In *S. aureus*, it was initially shown that the membrane-associated protein elastin binding protein EbpS promotes binding of soluble elastin peptides and tropoelastin to the bacteria and suggested that EbpS might be the adhesin responsible for the bacterial colonization of elastin-rich tissues. Although it promotes binding of soluble elastin peptides and tropoelastin to *S. aureus* cells, it is not able to promote bacterial adherence to immobilized elastin (Park *et al.*, 1999) (Downer *et al.*, 2002). In a later study, a major role as elastin-binding protein was attributed to FnBPA and FnBPB (Keane *et al.*, 2007). Knowing the similarities between those adhesins and SpsD/L (Figure 8), it is very likely that SpsD and SpsL bind to elastin. Indeed, SpsD (36% of identity with FnBPB) has been reported to bind elastin *in vitro* through its N2-N3 subdomains (Pietrocola *et al.*, 2013) following an uncertain mechanism. These results were obtained performing ELISA type ligand-binding assay and confirmed by Western ligand blotting. Concerning SpsL, the binding has not been described but adhesion between other bacterial adhesins such as *S. aureus* FnBPB (27% of identity with SpsL) and elastin (Roche *et al.*, 2004) leads to believe that the SpsL-elastin interaction is effective.

2. AFM, a window towards virulence mechanisms

This section will introduce atomic force microscopy (AFM), a powerful and versatile toolbox at the heart of this thesis, to notably study receptor-ligand interactions at the single molecule level. After briefly introducing its history (2.1) and basic principle (2.2), the AFM diverse operating modes will be described (2.3) with a particular attention to force spectroscopy (2.4) which allows probing specific molecular interactions, in addition to the classical topographic imaging capacities of such instrument.

2.1 Historical perspective

To cope with the lack of resolution due to diffraction issues of classical optic microscopy, electronic and near-field scanning microscopies have emerged during the 20th century. The AFM enables to reach the nanoscale, even to the atomistic level (Figure 12), has been introduced in 1986 by Binnig *et al.* as a solution to the limitations of scanning tunnel microscope (STM) concerning biological systems analysis (Binnig *et al.*, 1982), (Binnig *et al.*, 1986). Indeed, the STM technology consists in scanning a surface with a metallic conductive tip at constant tunnel current taking advantage of the tunneling effect enabling electrons to move from a conductive substrate to the sharp tip when the distance between the two objects is smaller than 1 nm, creating a measurable current called the "tunneling current". The displacement of the tip gives a topographic picture of the surface because the height of the tip is constantly adjusted as a function of the tunneling current. However, this technique presents two major limitations: the surface has to be conductive in order to be imaged and the experiment has to be carried out under a high vacuum. Those conditions are obviously not suitable for living biological systems since first, as vacuum is necessary, it is not suited to visualize living samples, and secondly electron beam focused on the sample can damage it.

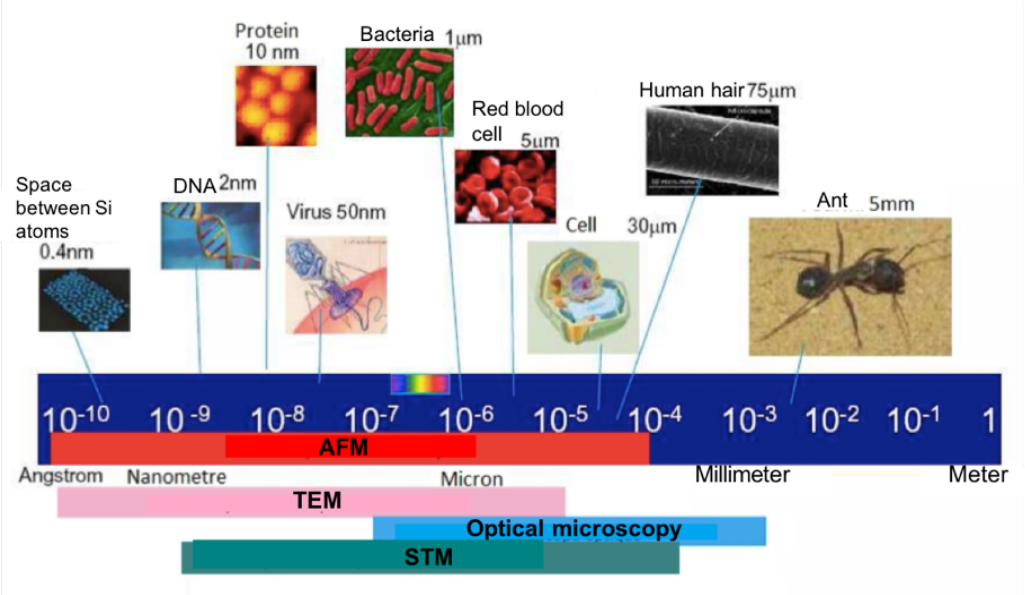

Figure 12: Field of use of microscopic observation techniques. TEM: Transmission Electron Microscopy.

In order to avoid those issues, the AFM does not rely on tunneling current, as the STM, but on the measurement of local interactions forces (attractive and repulsive intermolecular forces) between a probe and a sample surface, which does not require neither vacuum nor a (semi)conductive surface/sample. Since its invention as a pure imaging technique, AFM has evolved as a versatile toolbox, also able to quantitatively map various physical, chemical and biophysical properties (such as adhesion, elasticity or deformation) of the sample, with high spatiotemporal resolution and high force sensitivity (Dufrêne *et al.*, 2013). This technique is applicable on various samples, such as synthetic polymers or biological material and allows to investigate the dynamics of the studied processes under physiological conditions if needed (Dufrêne, 2008).

2.2 Setup

In a classical AFM imaging configuration, a laser beam is reflected on the extremity of a sharp tip located at the end of a soft cantilever onto a photodiode. The interactions between the tip and the sample surface are measured based on this deflection monitored via the laser beam reflected (Figure 13). Depending on the sample topography and the interactions between the sample and the tip, the cantilever is attracted or repulsed from the surface. A piezo electric scanner placed either in the AFM head or under the sample controls the movements of the cantilever or the sample in the scale of the nanometer. The scale of measurement varies from the single molecule to the study of entire living cells, with a lateral resolution of 1 nm and a vertical one of 0.1 nm (Müller *et al.*, 2009). The force sensitivity being in the piconewton (pN) range, allows the measurement of inter- and intramolecular forces (Radmacher, 2002).

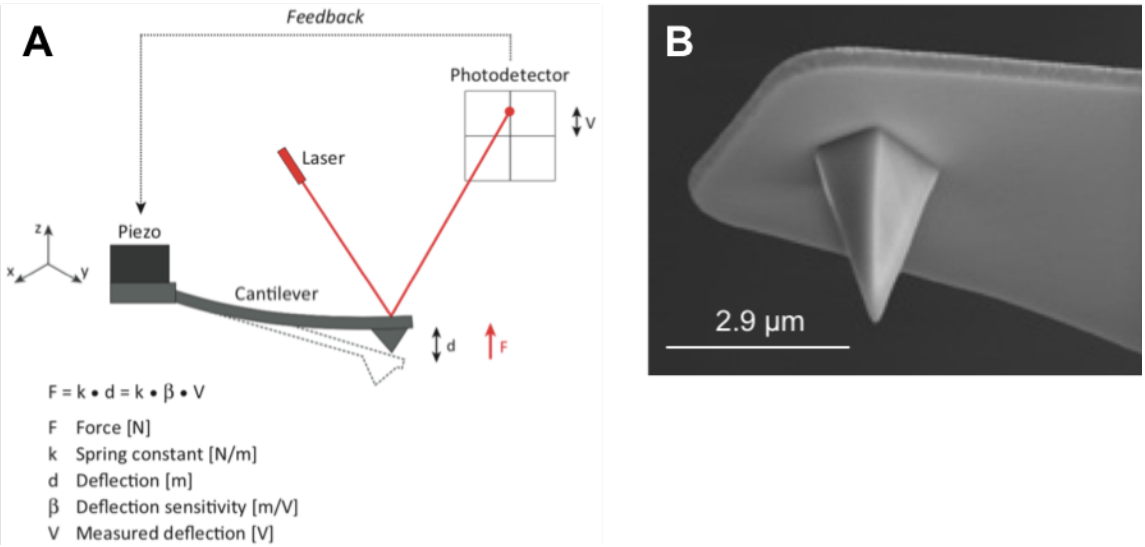

Figure 13: Schematic representation of an atomic force microscope (left) and SEM imaging of a probe (cantilever and tip) (right). Forces affecting the cantilever tip cause bending of the cantilever, measured via the reflection of a laser beam onto a photodetector constituted of 4 photodiodes. An x-y piezoelectric scanner allows for scanning the tip over a sample, whereas a z-piezo and a feedback system enable vertical tip position control. The force F exerted on the tip is related to cantilever deflection d and spring constant k; the deflection is measured in volts V, and the deflection sensitivity ß converts it from volts to meters (Guillaume-Gentil et al., 2014), (Bruker internet site: https://www.brukerafmprobes.com/p-3419-msct.aspx).

The cantilever acts as a spring near the surface of the sample. Its movements can be described by Hooke's Law:

$$F = k.d$$

where k is the spring constant of the cantilever and d is the deflection of the laser beam on the photodiode. This equation links the force between the tip and the sample to the deflection of the cantilever. The desired raw data consists of voltage-distance curves (see section 2.4), but since the recorded parameter is the voltage variation on the photodiode, it is needed to convert them using two intrinsic parameters of the AFM cantilever, sensitivity and spring constant (Figure 13) as shown in the following equation:

$$F = k.\beta.V$$

where β is the deflection sensitivity and V is the measured voltage. The deflection sensitivity β [m/V] is measured thanks to the force-distance curve of the tip against a firm surface. It corresponds to the slope of the retraction curve and allows converting the observed voltage deflection on the photodiode in Volt (V) into the cantilever deflection in meter (m). The spring constant k [N/m] allows the transformation of the cantilever deflection into forces via Hooke's law and is generally obtained by the Thermal noise method (Hinterdorfer and Dufrêne, 2006).

The topographical feature of the sample can be obtained following different operating mode based on the movements described by the tip. Those modes were developed and improved to reduce sample damages and increase spatial and time resolution, as well as force sensitivity. Three modes can be distinguished that will be briefly described thereafter: contact mode, non-contact mode, and tapping or dynamic mode.

2.3 Operating modes

- Contact mode

In contact mode (Figure 14 left), the tip is in permanent contact with the sample, moving laterally line by line, assembled to create a height map of the sample surface. In this mode, deflection of the cantilever has to remain constant, so the force applied to the surface is kept constant by continually adjusting the height of the cantilever through a retroaction loop. The feedback loop acts to move the sample vertically in order to bring back the deflection to the set point value and thus keeps the force acting on the sample constant. The result is a topographic map of the sample corresponding to the movement of the piezoelectric scanner. The resolution depends on the structure of the AFM tip, the sample roughness, the physical properties of the sample and the precision of the feedback loop of the piezo-scanner (Dufrêne *et al.*, 2017). This method is however difficult to carry out on biological samples while keeping their surface intact due to the force applied on it.

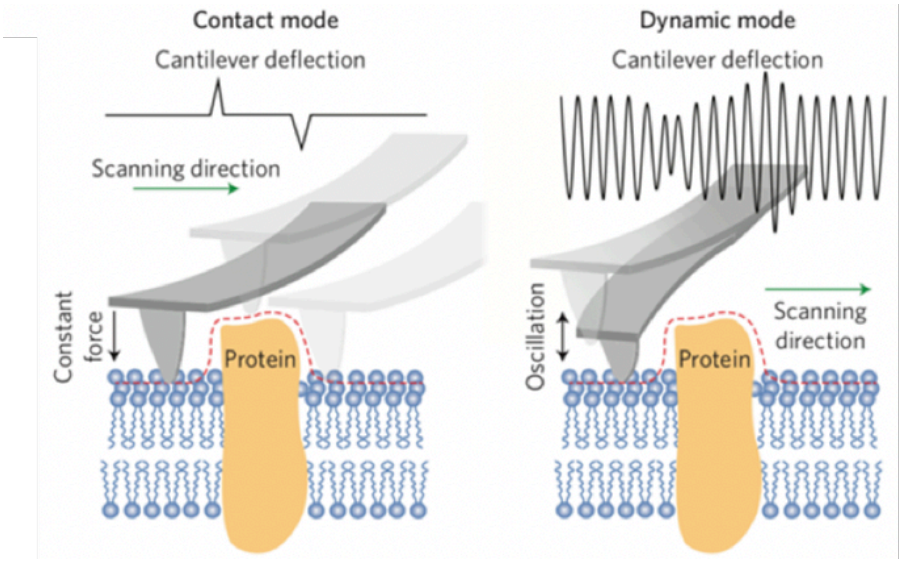

Figure 14: AFM-based imaging of biological systems with molecular resolution. The contact mode (left) consists of a constant force applied to the sample; any topographic change modifies the cantilever deflection and the tip-sample distance is constantly adapted by a retro-action loop. The Dynamic mode (right) consists of an oscillation of the cantilever at or near its resonance frequency over the sample and any variation of the sample topography modifies the oscillation leading to an adjustment of the tip-sample distance (Dufrêne et al., 2017).

- Non-Contact mode

In non-contact mode, the tip is moved close (order of Angstroms) to the surface of the sample, the probe is then scanned across the surface, and the image is constructed from the force interactions during the scan. During measurements the tip is driven so that it oscillates. The force interactions are measured either by measuring the change in amplitude of the oscillation at a constant frequency near resonance frequency (amplitude modulation) or by measuring the change in resonant frequency directly using a feedback loop to always drive the tip on resonance (frequency modulation). Therefore, by monitoring either the vibrational amplitude or the resonating frequency of the cantilever, and by keeping this constant using a feedback loop that continuously adjusts the height of the tip, a topographical image of the sample can be obtained. Understandably, tip and sample degradations are in general faster in contact mode than in non-contact mode (Smallman and Ngan, 2014).

- Tapping mode

A hybrid mode between the contact and non-contact modes can also be performed. This is known as tapping mode, or dynamic mode (Figure 14 right). The tapping mode is very similar to non-contact mode, except that the vibrating tip is brought closer to the sample, so that it barely hits, or 'taps', the sample (Smallman and Ngan, 2014). The tapping mode has been developed in order to minimize the friction between the tip and the sample observed in contact mode (Dufrêne *et al.*, 2017). By reducing the lateral forces, the tapping mode allows the study of systems that are poorly adsorbed on the surface, objects that are rougher or soft biological samples (Dufrêne *et al.*, 2017). In this case, the cantilever is driven at a constant frequency near

resonance and the force variations can be detected either as a variation in the amplitude or in the phase of the cantilever vibration (Albrecht *et al.*, 1991).

2.4 Force spectroscopy

2.4.1 General principle

In addition to its imaging capacities, AFM can be used to obtain quantitative measurements of the force involved in the interaction between the tip and the sample as a function of the distance between them, in the so-called force spectroscopy mode firstly developed in 1989 by Weisenhorn *et al.* (Weisenhorn *et al., 1989*). In this mode, the tip approaches the surface gradually with controlled increment steps until contact is achieved and then retracts, while recording the movement. Consequently, while the cantilever performs those approach-retract cycles from the surface, a force-distance curve (FD) is obtained by monitoring the deflection of the cantilever as a function of the vertical displacement of the piezoelectric scanner.

Force-distance curves can be described as follow (Figure 15):

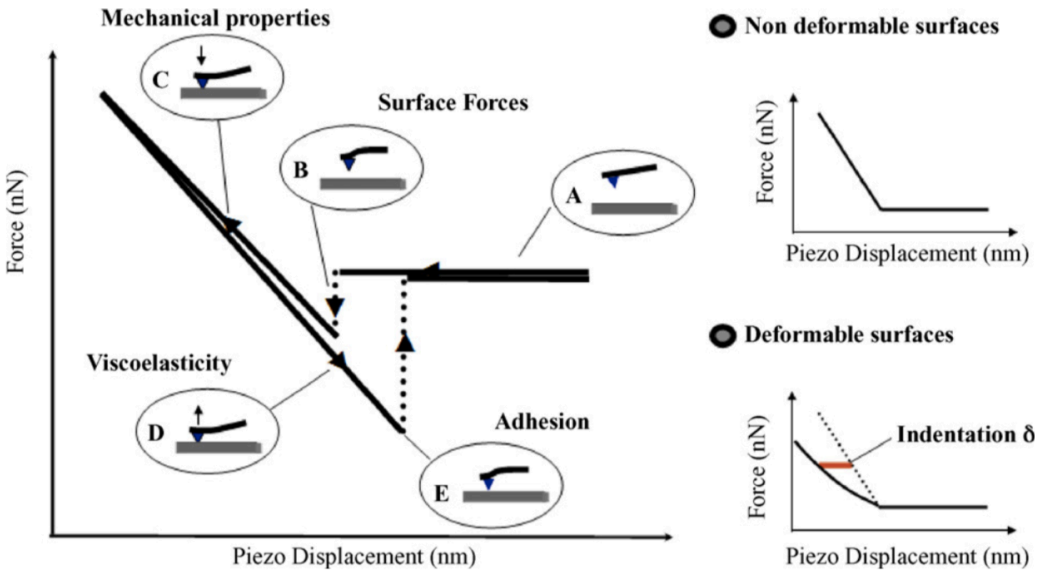

Figure 15: Schematic diagram of a typical force curve for a non-deformable surface with attractive forces between the AFM probe and the sample (Left). The two ideal diagrams on the right show the approach force curves for non-deformable (top) and deformable (bottom) samples in the absence of surface forces (Gaboriaud and Dufrêne, 2007).

(A) During the approach, the tip is lowered to the surface of the sample. (B) In case of van der Waals attractive interactions between the tip and the surface, the cantilever bends downwards. (C) Once the tip is close enough, it enters in contact with the surface and the cantilever bends upwards until a pre-defined setpoint of vertical deflection is reached. (D) After a defined time of contact, the cantilever retracts from the surface and (E) in the case of an adhesive event, a hysteresis between the approach and the retract is observed. Finally, the tip reaches back its

resting state (baseline, zero force). The shape of the curve depends on the affinity of the sample for the tip but also on the deformability of the surface. When the surface is soft, an indentation during the approach is observed (Figure 15, bottom right) (Gaboriaud and Dufrêne, 2007).

These force-distance curves provide the required distance (on the x-axis) and force (on the y-axis) needed to effectively unbind the sample and the probe (if adhesion occurs), called respectively rupture length and adhesion force.

From such curves, along with tip-sample adhesion, other various biophysical properties can be extracted, including stiffness, elasticity (Young's modulus), energy dissipation (Figure 16) (Gaboriaud and Dufrêne, 2007).

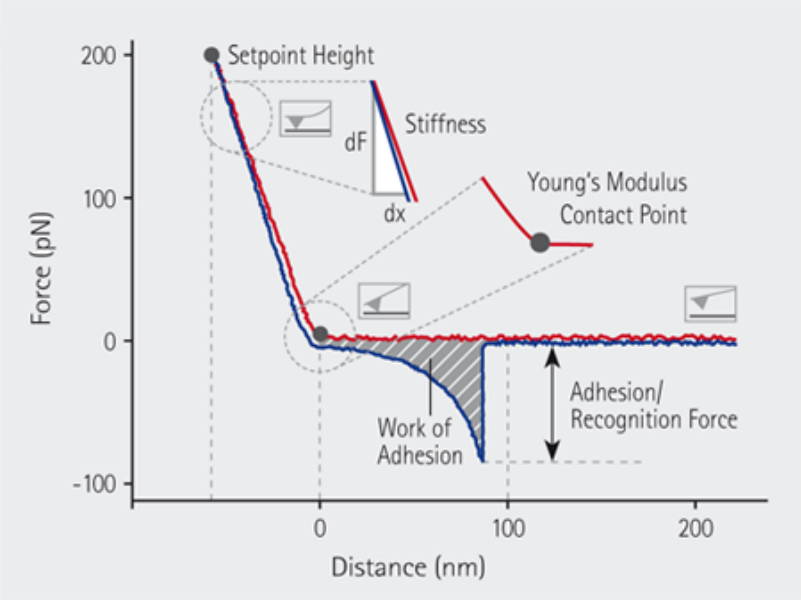

Figure 16: Schematic diagram of a typical specific force curve and various biophysical properties deduced from the curve. Approach in red and retract in blue (JPK internet site: https://www.jpk.com/products/atomic-force-microscopy/qi-mode).

2.4.2 Single Cell and Single Molecule Force Spectroscopies

The force spectroscopy method depicted above uses bare AFM tip. But it is also possible to modify and functionalize the tip. Two major techniques derive from these modifications: single cell force spectroscopy (SCFS) and single molecule force spectroscopy (SMFS). Both technics consist in functionalizing the tip with one of the two partners (either the ligand or the cell) and probe the interaction with the complementary partner which is fixed on a support. Briefly, in SMFS, AFM tips labeled with cognate ligands are used to detect, localize, and manipulate individual receptors, whereas in SCFS, the tip is replaced by a living cell to measure single-cell adhesion forces (Figure 17). Both approaches provide a wealth of information on the strength, specificity, and dynamics of microbial cell surface interactions (Mathelié-Guinlet *et al.*, 2019), (Viela *et al.*, 2020 a).

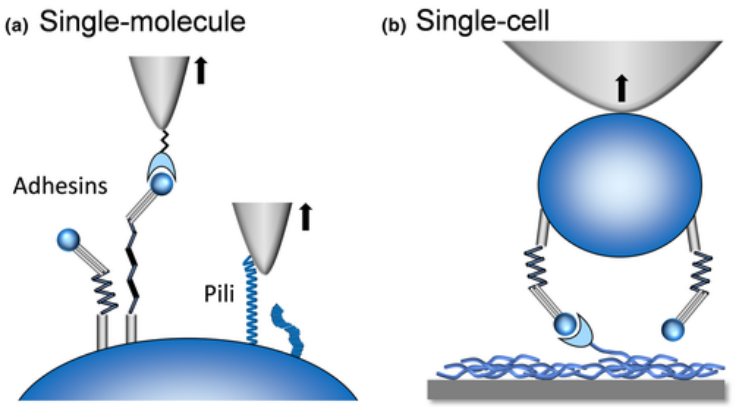

Figure 17:Cantilever set up in SMFS and SCFS. In single-molecule force spectroscopy (SMFS; a), AFM tips labelled with cognate ligands are used to force probe individual components like adhesins and pili, while in single-cell force spectroscopy (SCFS; b), the tip is replaced by a living cell in order to measure single-cell adhesion forces towards solid substrates, ligands or other cells (Viela, 2020 a).

2.4.3 AFM tip functionalization

- Single cell force spectroscopy (SCFS)

In SCFS, a tipless cantilever is functionalized with a single living cell (Figure 17b). For the fixation of the cell, different methods are used such as receptor ligand interactions, electrostatic interactions, glue or chemical fixation (Hinterdorfer and Dufrêne, 2006). The attachment of the cell should not only preserve the metabolic activity and the natural surface architecture of the cell but also be stronger that the interaction probed towards the sample in order to remain unbroken at the end of the experiment.

Yves Dufrêne team has developed a versatile and reliable fixation method to comply with such criteria (Figure 18). They first attach a colloidal silica bead at the apex of the tip-less cantilever through UV-curable glue. Then, by further coating this bead with polydopamine, a single living cell can finally be immobilized by simple contact (Beaussart *et al.*, 2013). This method is nondestructive and offers a good control of the contact area, which gives the possibility of reproducible single cell analysis (Dufrêne, 2015).

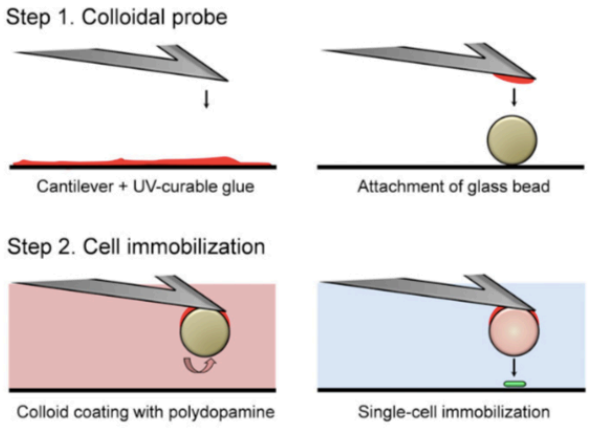

Figure 18: Single-bacterial cell force spectroscopy using colloidal probe cantilevers combined with bioinspired polydopamine polymers. The method involves two main steps, i.e., preparation of the colloidal probe and controlled immobilization of a single cell on it (Beaussart et al., 2013).

- Single molecule force spectroscopy (SMFS)

In SMFS, the tip of the cantilever is functionalized with molecules of interest for the study and then probed against the cell immobilized on a support (Figure 17a). Just like SCFS, some factors have to be considered to achieve optimal detection. First, the binding of the molecule on the tip has to be much stronger than the molecular forces studied. Consequently, rather than physical adsorption, a direct covalent binding to the tip is the best way to cope with such requirement as covalent bonds are much stronger than typical receptor-ligand bonds (~hundreds of pN). Second, the density of grafted molecules on the cantilever has to be low to ensure single molecule interactions. Third, it is also important to limit non-specific interaction, respect the orientation of the molecule (which can be important and can be controlled in some cases) and sometimes use a flexible molecular spacer that allows the molecule to freely interact (Hinterdorfer and Dufrêne, 2006).

Concerning the grafting, the biomolecules can be attached on a gold-coated tip via self-assembled monolayers (SAMs) of functionalized alkanethiols. The end-groups of the alkanethiols will react with the compound of interest. Alkanethiols with carboxyl functional groups are activated with a solution of NHS/EDC (N-hydroxysuccinimide (NHS); 1-ethyl-3-(3-dimethylaminopropyl)- carbodiimide (EDC)) and are able to form covalent bonds with the amine groups of the compound of interest (Figure 19) (Ebner *et al.*, 2007). The same procedure can be achieved on gold supports when ligands need to be immobilized for SCFS experiments. While SCFS probes adhesive forces of whole cells, SMFS captures the binding force and dynamics of single adhesins.

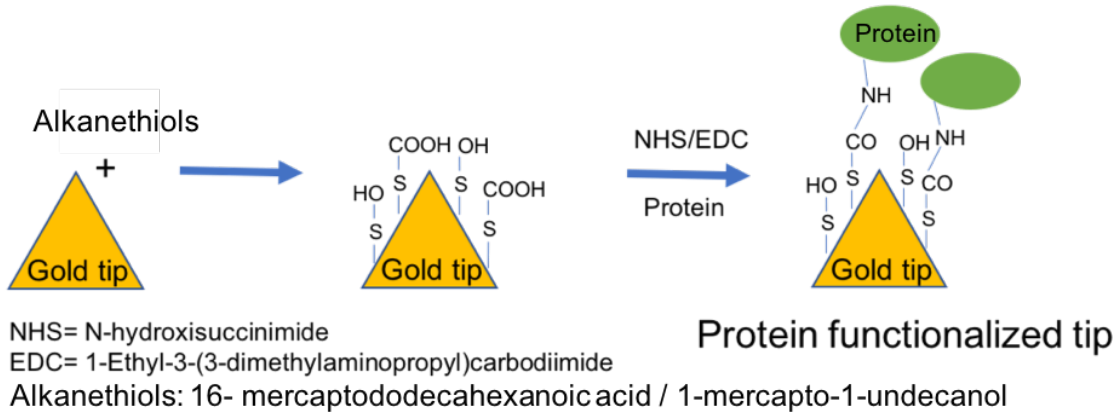

Figure 19: Steps of SMFS gold tip functionalization. A gold tip is grafted with alkane thiols. Thiols with carboxyl functional groups are activated with a solution of NHS/EDC (N-hydroxysuccinimide (NHS); 1-ethyl-3-(3- dimethylaminopropyl)- carbodiimide (EDC)) and are able to form covalent bonds with the amine groups of the protein (in green).

2.4.4 Force-distance based AFM imaging

Noteworthy is the existence of an AFM multiparametric (or force-distance based) imaging mode which combines surface imaging and force spectroscopy, namely Quantitative Imaging (QI) in JPK standard and PeakForce tapping in Bruker one. By recording pixel-by-pixel a whole array of FD curves over the sample, this mode allows imaging a biological system while simultaneously mapping the physical/mechanical properties (adhesion, stiffness…) of the system with piconewton sensitivity and at a high spatio-temporal resolution (Figure 20). This mode allows the correlation between the interactions and the topography of the sample, especially interesting when tips are grafted with cognate ligands (Dufrêne *et al.*, 2013).

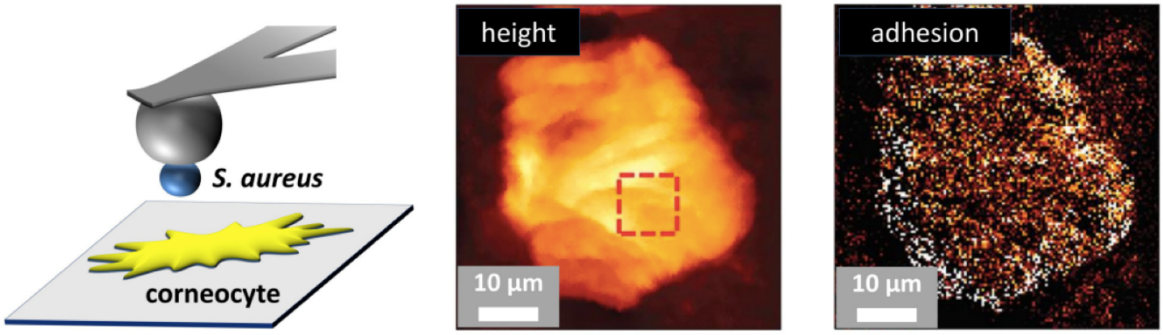

Figure 20: Quantitative Imaging used in combination with SCFS and single S. aureus cell-probes vs corneocytes cells (Viljoen et al., 2020).

Another quantitative imaging mode, extensively used notably in Yves Dufrêne lab, is the so-called force-volume (FV) imaging mode. It is performed across a square area of the surface sample recording typically 32 x 32 curves (within ~ 25 min depending on the pulling speed). Although powerful, the FV mode faces some limitations concerning the increase of the lateral resolution being time consuming (64 x 64 curves within 80 min). Moreover, this increase in resolution can lead to an excessive thermal drift during which the scanned area stays no longer the defined one.

3. Objectives and strategies

Considering the emergence of zoonosis cases for *Staphylococcus pseudintermedius* and the increasing occurrence of methicillin-resistant strains, it is now crucial to unravel the mechanisms by which such pathogens adhere to-, and in turn infect, their hosts, including the fundamental proteins of the ECM. Unlike ensemble techniques, the AFM (especially SMFS and SCFS) allows to quantify, at the molecular level, the adhesion forces between such pathogens and cognate ligands, with unprecedented spatiotemporal resolution. Thus, the main objective of this work will be to characterize by AFM means the interaction of *Staphylococcus pseudintermedius* adhesins SpsD and SpsL with elastin.

Previous researches using AFM and lead by Yves Dufrêne team reveled some of the features involved in the interactions between Sps adhesins and ECM ligands (Fn and Fg). Concerning the Sps-Fn interaction: while SpsL binds to Fn with low forces of ~ 200 pN, SpsD -Fn interactions feature forces > 1,5 nN, suggesting that the two adhesins of *S. pseudinermedius* are engaged in two modes of interaction with Fn. Based on the dynamical investigation of these interactions and the structure of the proteins, they also argue that the strong SpsD-Fn interaction results from the β-sheet organization of a mechanism called "tandem β-zipper", reminiscent of that occurring in *S. aureus* FnBPs (Viela *et al.*, 2020 b). Moreover, Mathelié-Guinlet *et al.* demonstrated that the interaction between SpsD and Fg was also extremely strong featuring forces > 1,5 nN and mechanically activated, high forces being favored at large stress. This strong interaction originates from a "dock, lock and latch" (DLL) binding mechanism (further discussed in section 5.5) which appear to be the first catch bond revealed on living bacteria (Mathelié-Guinlet *et al.*, submitted).

In this context, I started my memoire in Yves Dufrêne team to further the knowledge on the SpsD/L interactions with ECM ligands, especially focusing on elastin. Quantification of the forces involved in the binding of these adhesins to elastin and the dynamics of these interactions under mechanical force will be investigated in order to understand the underlying mechanisms of these interactions.

4. Material and methods

4.1 Bacterial cells, culture conditions and proteins

S. pseudintermedius strain ED99 was isolated from a canine bacterial pyoderma case. Mutant strains were designed by our collaborators, following the method described in Pietrocola *et al.*, 2015 (Pietrocola *et al.*, 2015), to obtain ΔspsL, ΔspsD and ΔspsDΔspsL, respectively called SpsD, SpsL and double mutant cells in this manuscript. From such cryostocks (kept at -80°C), bacterial plates brain heart infusion (BHI agar) were made by stroking some bacteria all over the plates which are then incubated overnight in an incubator at 37°C for the colonies to grow. Cells were grown in BHI broth (one colony for 10 mL) overnight, at 37°C and under shaking at 200 rpm, to reach their stationary phase. The day of experimentation, cells were harvested by centrifugation at 3000 g for 5 minutes, washed twice with Phosphate buffer saline (PBS) and resuspended in PBS. Finally, a 100x dilution was prepared and used for experiments. α-elastin, a mixture of soluble peptides obtained from human lung (Calbiochem, Merck, Darmstadt, Germany) stored at -20°C after aliquotation (50 µL at a concentration of 0.1 mg/mL) and used directly without further manipulation.

4.2 Atomic force microscopy experiments

Before the actual experiment, the AFM is set up as following: First the cantilever, functionalized depending on the experiment nature (see sections 4.2.1 and 4.2.2), is mounted in the AFM head maintained in a glass block. Then the AFM petri dish supporting ether the ligand, or the bacteria is mounted on the piezoelectric scanner in the slot provided. The laser is then focused on the cantilever and the signal is maximized by adjusting the positions of both photodiode and mirror (Figure 13, see section 2.2). Finally, we carry out the calibration as previously described (see section 2.2) in order to determine the sensitivity and the actual spring constant of the cantilever.

4.2.1 Functionnalization of gold tips and surfaces

Gold cantilevers used for SMFS experiments (OMCL-TR400PB-1, Olympus Ltd., Tokyo, Japan) were first rinsed with ethanol, dry with a nitrogen flux and placed in UV-ozone for 15 min. to remove all organic matter. Then, they were immersed overnight in an ethanol solution containing 1 mM of 10% 16- mercaptododecahexanoic acid / 90% 1-mercapto-1-undecanol (Sigma). After being rinsed with ethanol and dried with N_2, they were then immersed for 30 min into a solution containing 10 mg/mL N-hydroxysuccinimide (NHS) and 25 mg/mL 1-ethyl-3-(3- dimethylaminopropyl)-carbodiimide (EDC) (Sigma). Finally, after being rinsed with

ultrapure water, they were incubated with 0.1 mg/mL of α-elastin for 1 h, rinsed further with PBS buffer, and then immediately used without de-wetting.
The exact same protocol was followed for gold surfaces (mica coated with a thin layer of gold) used in SCFS experiments.

4.2.2 Preparation of colloidal probes for SCFS experiments

As before any experiment, NP0-10 cantilevers (Bruker) were washed with ethanol, dried with nitrogen and finally cleaned for 15 min under UV-Ozone-cleaner. Tip-less cantilevers chosen for SCFS experiments were relatively stiff, with a nominal spring constant of 0.6 N/m, to allow the immobilization of a colloidal silica microsphere at its end. To do so, a glass slide was prepared with UV-curable polymer on one side and silica beads (6 µm diameter, provided as a powder) on the other side. Using a Nanowizard III AFM coupled to an optical microscope, it was then possible to (i) incrementally approach the cantilever to the uv-curable polymer until it touches it and becomes covered, and then (ii) move the cantilever to the location of a bead and catch it at its extremity by a similar manual approach. After this procedure, the newly made colloidal probes were exposed to UV-light for 15 min to cure the polymer and fixed the bead to the cantilever.

4.2.3 Implementation of Single Cell Force Spectroscopy (SCFS) experiment

Before any SCFS experiment, the colloidal probes were immersed for at least 1 h in Tris Buffer Saline (TBS) (pH = 8.5) containing 4 mg/ml of dopamine hydrochloride, then rinsed in TBS (3x). This step will allow to catch a negatively charged bacteria by electrostatic interactions. Before any manipulation, the cantilevers were calibrated in order to measure their sensitivity and their spring constant by the thermal noise method, as explained previously. The experimental set up of SCFS consisted of a polystyrene petri dish, where a drop of *S. pseudintermedius* suspension is deposited near a gold support functionalized with α-elastin (as described in 3.2.1) which is never allowed to dry. Cells are let ~ 30 min to settle and the dish is rinsed twice with 1 mL of PBS, and then filled with 2mL of PBS. Before performing FS, a cell was first immobilized on the colloidal probe by approaching the cantilever to an isolated cell and waiting 5 sec when the contact point was reached before retracting the tip. Then, the cantilever was moved to the gold support coated with elastin, in order to probe its interaction with the single cell. The standard experimental parameters were: room temperature, applied force of 250 pN, a constant approach-retraction speed of 1000 nm/s. Adhesion maps on square areas of 5 µm x 5µm were obtained by recording a 16 by 16 pixels map in which a force-distance curve is recorded for each pixel. At least 6 cells of 2 independent cultures were probed, for each cell at least 2 maps on different areas were acquired.

4.2.4 Implementation of Single Molecule Force Spectroscopy (SMFS) experiment

For SMFS experiments, gold cantilevers (k ~ 0.02 N/m) were functionalized with α-elastin, as previously detailed. A drop of *S. pseudintermedius* solution is deposited in order to be immobilized on an AFM petri dish in polystyrene. After 30 min of incubation, the dish is rinsed twice with 1 mL of PBS, and then filled with 2ml of PBS. SMFS measurements were performed at room temperature in PBS buffer with a NanoWizard III (JPK Instruments). An optical microscope allowed us to localize a single cell on which a first rough map of 10 µm x 10 µm was done to confirm the presence of the cell below the tip. Successive zoom in were performed to correct for the drift and final adhesion maps were obtained by recording 32 by 32 force-distance curves on square areas of 0,25 μm^2 on top of the bacteria with an applied force of 250 pN, a constant approach and retraction speed of 1000 nm/s. For loading rate (LR) experiments, arrays of 16 by 16 or 32 by 32 force curves were recorded on 500 nm by 500 nm areas at increasing retraction speeds: 0.5, 1, 3, 5 and 10 µm/s. At least 13 cells of both SpsD and SpsL strains from 3 independent cultures were probed.

4.3 Data processing and analysis

For both SCFS and SMFS, we were interested in the adhesion properties of the SpsD / SpsL - elastin complex. Adhesion forces and rupture distances, presented as histograms thereafter, were obtained by calculating the adhesion force and rupture distance of the last peak for each curve, pointing to the final unbinding of our system (Figure 21A). Other parameters were extracted from such curves. The spring constant of the molecular complex (K_m) was determined using the slope of the linear portion of the force vs tip position curves (Figure 21A). We have also determined the effective loading rate which was estimated for each FD curve from the force vs time curves. The LR corresponds to the load (the force) applied on the receptor-ligand bond over time (Figure 21B).

Raw data were analysed by the JPK data analysis software. With this software every curve of spectroscopy analysis was reviewed by the operator with a semi-automatic process taking into account the tip calibration (spring constant and the sensitivity), and the baseline level defined by the operator. The rupture length of the last peak and its corresponding force of adhesion were considered. The output file could be read by Origin pro (OriginLab) in order to extract the rupture length and the maximal adhesion of each curve and to compute the adhesion force and rupture distance histograms of each cell.

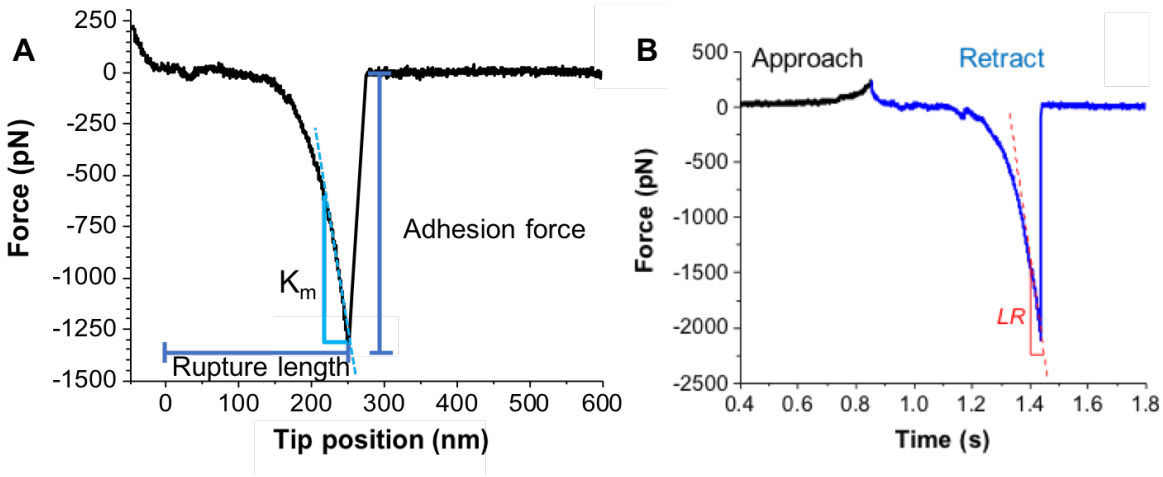

Figure 21: Example of a FD curve (and derivatives) and properties deduced from it. (A) Force-time curve displaying the measurement of adhesion force, rupture length and spring constant of the molecular complex (K_m). (B) Force-time curve displaying the measurement of the loading rate (LR).

5. Results and discussion

In this section, we will describe the role of SpsD and SpsL adhesins in the adhesion of *S. pseudintermedius* to elastin, investigated by means of both SCFS and SMFS. For more clarity, thereafter, we will refer to SpsL (SpsL$^+$ ED99) and SpsD (SpsD$^+$ ED99) cells respectively, thus emphasizing the presence of one of the adhesin rather than the absence of the other. We will first present the whole cell experiments results (4.1) and then focus on the strength of individual Sps-elastin bonds and their dynamics (4.2).

5.1 SpsD / SpsL -elastin interaction detected in SCFS

By means of SCFS, performed as described in Material and methods, the strength of interactions between SpsD or SpsL and human elastin was measured on living bacteria. We measured, in a first time, the binding forces between *S. pseudintermedius* SpsD cells and elastin (Figure 22).

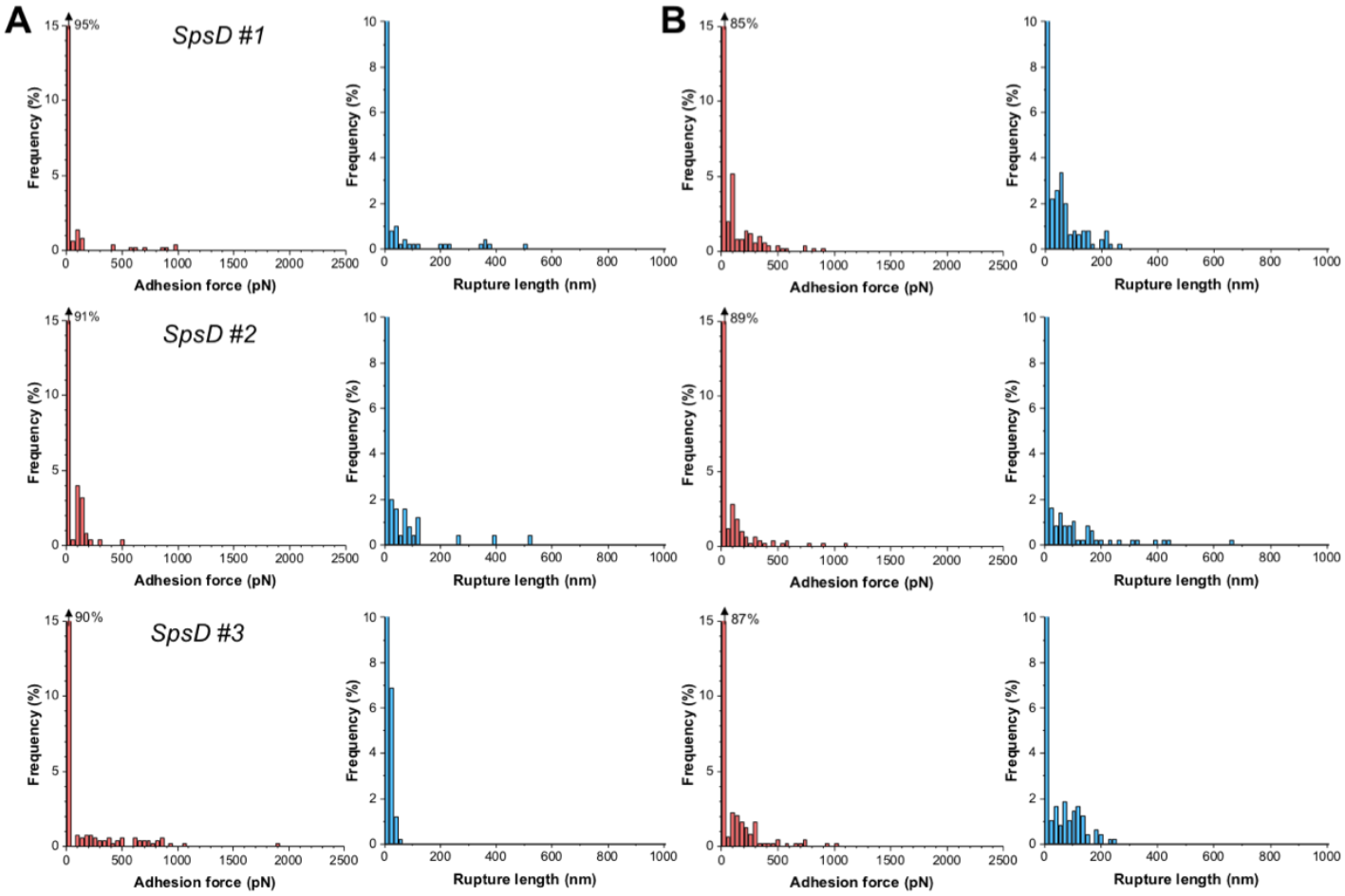

Figure 22: Adhesion forces between single SpsD cells and elastin substrates. Maximum adhesion force (in red) and rupture length histograms (in blue) obtained by recording force-distance curves in PBS between three representative S. pseudintermedius SpsD cells and elastin substrates at two different dwell times, 0 ms (A) and 500 ms (B). Percentages shown in adhesion histograms stand for the non-adhesive events (being the same for the rupture length histograms, they are not duplicated).

For the three representative SpsD cells shown in Figure 22, without any additional / imposed contact time between cell probe and elastin-surface, only a minority of FD curves exhibited adhesion events (5%, 9% and 10% for cell #1, #2 and #3 respectively). Adhesive events were weak in magnitude and broke at short (< 200 nm) rupture length. A binding probability of ~12% is observed over 7 independent SpsD cells (Figure. 23). This low biding probability, as compared to other reports in SCFS for *e.g.* SpsD-Fn interaction (Viela et al., 2020 b) might be due to the low contact time, *i.e.* the interaction between SpsD and elastin needs more time to be established. Thus, we performed the same experiments increasing the dwell time to 500 ms (Figure 22B). Similar adhesion profiles were observed with adhesion forces < 500 pN and short rupture lengths < 200 nm. We obtained an adhesion probability of ~17% (n = 6 cells) (Figure 23), which remains quite low compared to studies previously performed by the team.

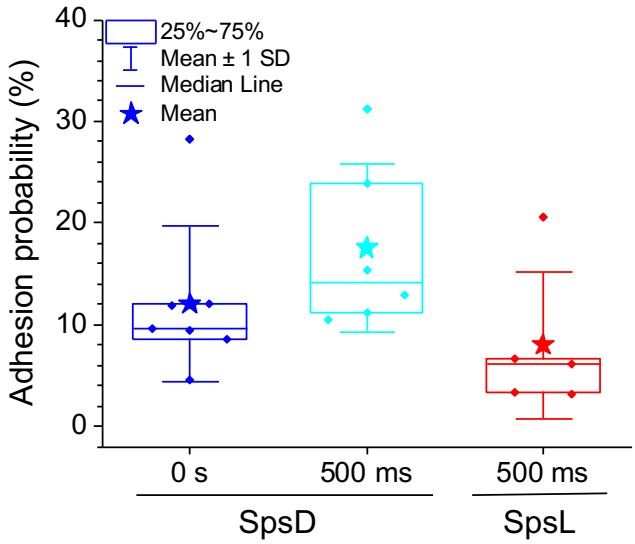

Figure 23: Probability of adhesion between SpsD or SpsL cells and elastin, obtained by SCFS.

We measured then, the binding forces between SpsL cells and elastin (Figure 24) with a dwell time of 500 ms. Though SpsL-elastin bonds lead to similar adhesion profiles than SpsD with observed adhesion forces < 500 pN and short rupture lengths < 200 nm, the adhesion probability decreased to ~8% (n = 8 cells) (Figure 23).

Knowing the behavior of SpsD implied in interactions with other ECM compounds (such as Fn and Fg), those results were not expected. Indeed, it has notably been reported using SCFS, first that the force required to break the interaction between SpsD and Fn or Fg can reach up to 1,5 nN and second that the binding probability can reach up to 60% for Fn and close to 100% for Fg (Viela *et al.*, 2020 b), (Mathelié-Guinlet *et al.*, submitted). Moreover, the results characterizing the SpsD-elastin interaction obtained using SMFS presented afterwards suggest that the values obtained using SCFS do not depict the specific interaction between Sps and elastin. This inconsistency could be explained by the intrinsic nature of elastin, which tend to self-polymerize (Vrhovski et Weiss., 1998).

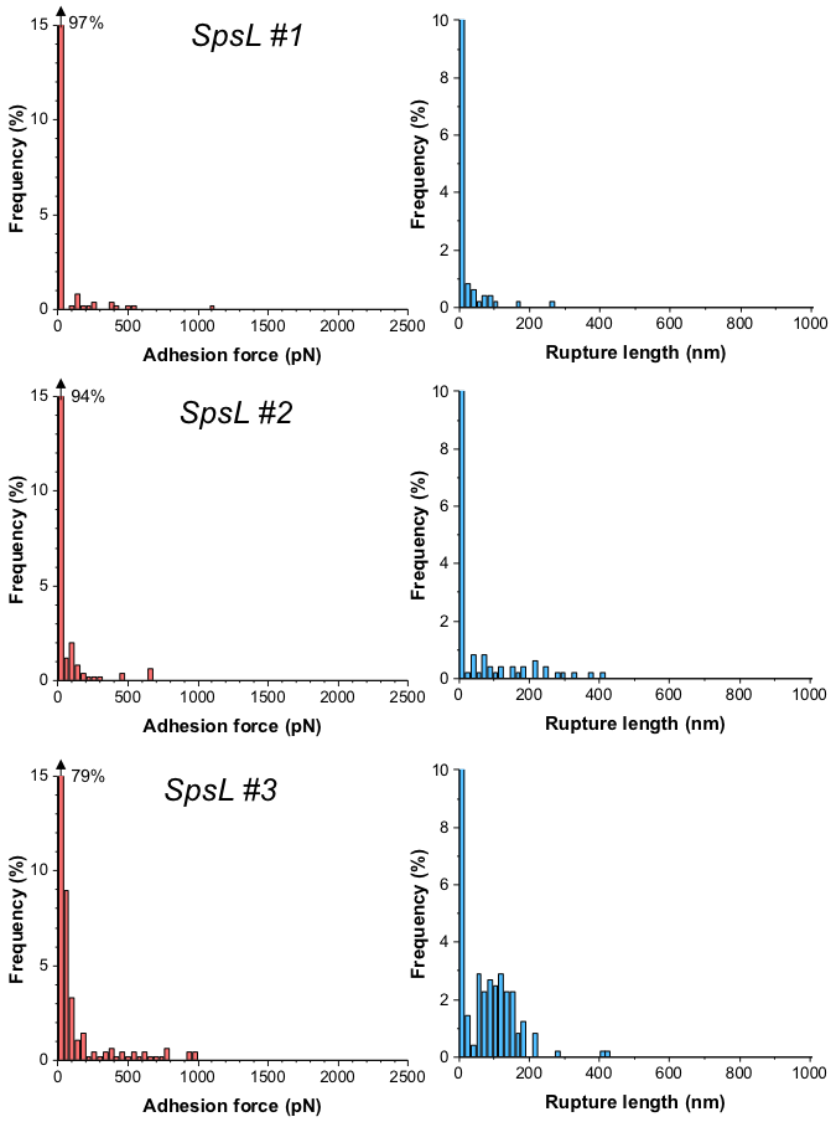

Figure 24: Adhesion forces between single SpsL cells and elastin substrates. Maximum adhesion force (in red) and rupture length histograms (in blue) obtained by recording force-distance curves in PBS between three representative S. pseudintermedius SpsL cells and elastin substrates at a dwell time of 500 ms.

Indeed, the elastin used in our experiments is α-elastin, a heterogeneous mixture of soluble peptides (60-84 kDa), having the capacity to reversibly coacervate under some conditions (Podrazky, 1967). The assembly required to perform SCFS involves the deposition of elastin molecules on a gold surface, forming a dense layer of ligands. The proximity created as well as the initial concentration of the elastin solution used would allow the aggregation of the molecules together during the use of the surfaces. Thus, the sites dedicated to the SpsD-elastin interaction would not be accessible to adhesin and the specific interaction would be compromised.

To overcome the issues revealed by SCFS experiments and quantify the molecular strength of SpsD and SpsL adhesins interacting with elastin, we then performed SMFS experiments. By functionalizing AFM tips with elastin, we aim not only at measuring the strength of single bonds but also at studying the dynamics of such interactions under force.

5.2 Two modes of interaction for SpsD and SpsL vs elastin highlighted by SMFS

Figure 25 presents the binding strength of four SpsD cells interacting with elastin. The results obtained on more cells are presented, as mean values, in Table 2.

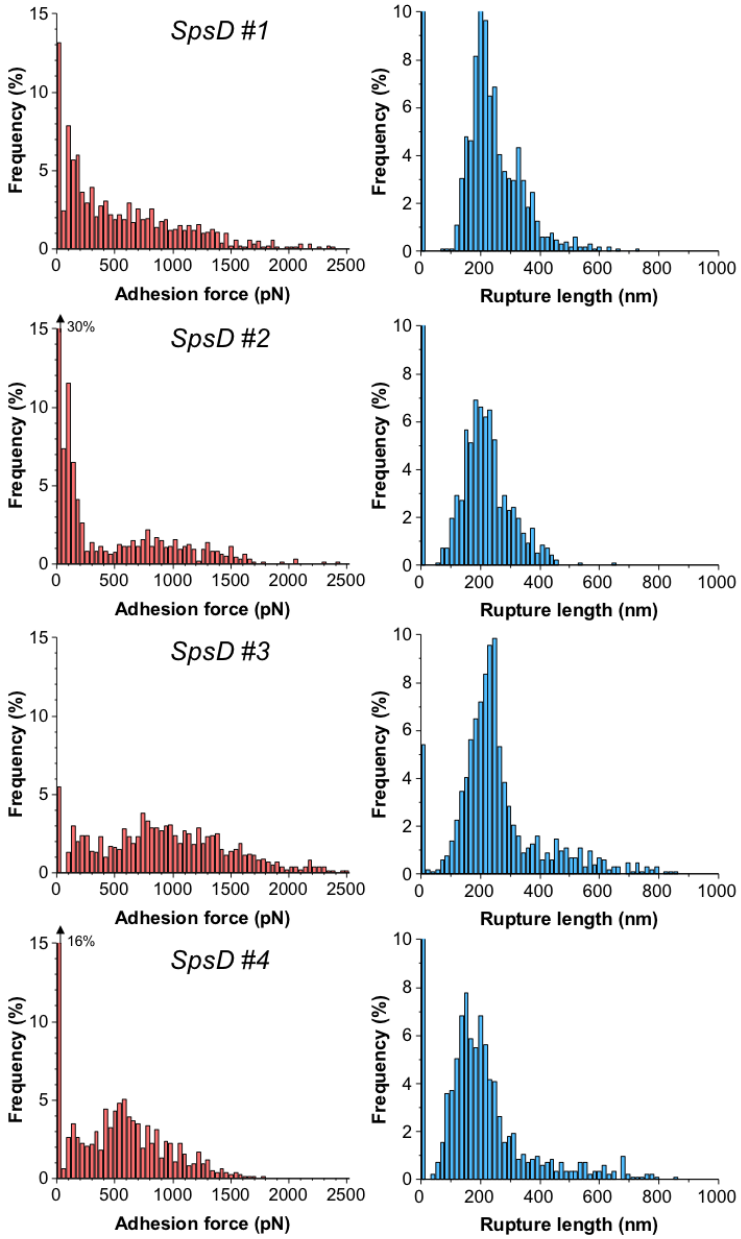

Figure 25: Binding strength of single SpsD-elastin bonds in living bacteria, obtained by SMFS. Maximum adhesion force (in red) and rupture length histograms (in blue) obtained by recording force-distance curves in PBS between four different S. pseudintermedius SpsD cells and AFM tips functionalized with elastin.

Force distributions featured adhesion events with both weak (< 500 pN) and strong (> 500 pN) forces, to an extent that varied from one cell to another. Analysis of the force profiles over the 14 cells yielded an average force of 207 ± 57 pN (mean ± standard deviation) in the low regime (n = 5191 total adhesive curves), while the high regime exhibited a mean of 1048 ± 204 pN (n = 4048 total adhesive curves) (Figure 26A). Noteworthy is the high adhesion probability ~68 % (n = 14 cells) displayed by SpsD towards elastin (Figure 26B).

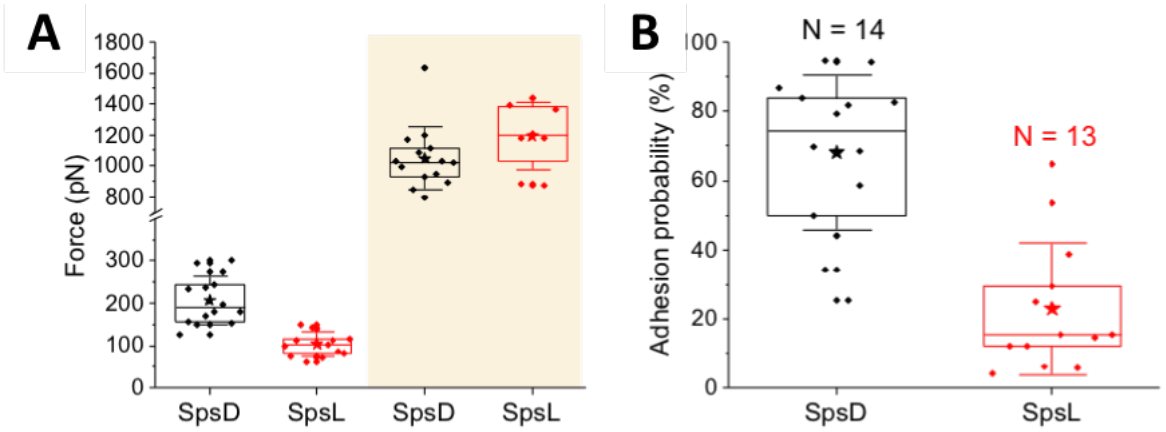

Figure 26: Statistical analysis of the binding capacities of SpsD and SpsL to elastin. (A) Average forces obtained in the low (white background) and high force regimes (orange background) for both SpsD and SpsL cells using SMFS. (B) Adhesion probability of SpsD and SpsL cells to elastin, obtained by SMFS. N stands for the number of independent cells studied. Stars represent the mean values, the box the 25%-75 % quartiles and the error bars the standard deviation among N independent cells.

The ~1 nN value (nearly equivalent to the strength of a covalent bond) exceeds by far the typical forces (~100 pN (Viela *et al.*, 2020 a)) involved in protein-ligand interactions. These ultrastrong forces have been previously reported for staphylococcal adhesins involved in a "dock, lock and latch" (DLL) interactions such as *S. epidermis* SdrG-Fg (Herman *et al.*, 2014) and *S. aureus* ClfA-Fg (Herman et al 2018) complexes. Considering that SpsD has already been reported to bind elastin through a variation of the DLL mechanism, our results are in good agreement with such model which involves dynamic conformational changes of the adhesin and results in an extremely strong adhesin-ligand complex (mechanism will be further discussed in section 5.5).

Table 2: Probability of adhesion (P_{adh}), adhesion force (F_{adh}) and rupture length (L_{rupt}) measured by SMFS between elastin-modified AFM tips and SpsD cells. The mean values are given with the corresponding standard deviation (mean ± s.d.).

	P_{adh} (%)	Low force regime < 500 pN						High force regime > 500 pN					
		F_{adh} (pN)			L_{rupt} (nm)			F_{adh} (pN)			L_{rupt} (nm)		
cell 1	79	179	±	101	209	±	91	928	±	399	218	±	91
cell 2	44	170	±	106	158	±	91	794	±	268	180	±	100
cell 3	50	197	±	101	370	±	161	1113	±	653	316	±	200
cell 4	82	244	±	123	393	±	193	1082	±	428	278	±	157
cell 5	26	236	±	121	280	±	178	1030	±	450	257	±	186
cell 6	95	275	±	117	331	±	187	1171	±	475	256	±	119
cell 7	94	296	±	124	376	±	189	1201	±	475	354	±	113
cell 8	84	300	±	136	270	±	175	844	±	272	213	±	118
cell 9	34	149	±	94	295	±	147	1631	±	576	291	±	114
cell 10	83	152	±	101	376	±	152	948	±	384	279	±	180
cell 11	87	232	±	125	271	±	105	1017	±	398	233	±	69
cell 12	70	155	±	101	221	±	85	1027	±	359	227	±	73
cell 13	59	180	±	118	210	±	99	997	±	351	214	±	76
cell 14	68	127	±	80	315	±	81	893	±	259	257	±	152

Similar bimodal force distributions were observed on SpsL cells (Figure 26A, 27, Table 3). Analysis of the force profiles over 13 cells yielded an average force of 104 ± 28 pN in the low regime (n = 2432 adhesive curves), while the high regime (only observed for 8 cells) exhibited a mean of 1189 ± 217 pN (n = 288 total adhesive curves). As clearly observed in Figure 27, though SpsL-elastin bonds feature both weak and high forces, the proportion of the latter is much lower than the former, which is eventually different from the SpsD-elastin interactions. Also, the adhesion probability dropped from 68 % to 23 % as compared to SpsD cells (Figure 26B), implying SpsL cells might adhere to elastin through similar mechanism than SpsD but to a much lower extent.

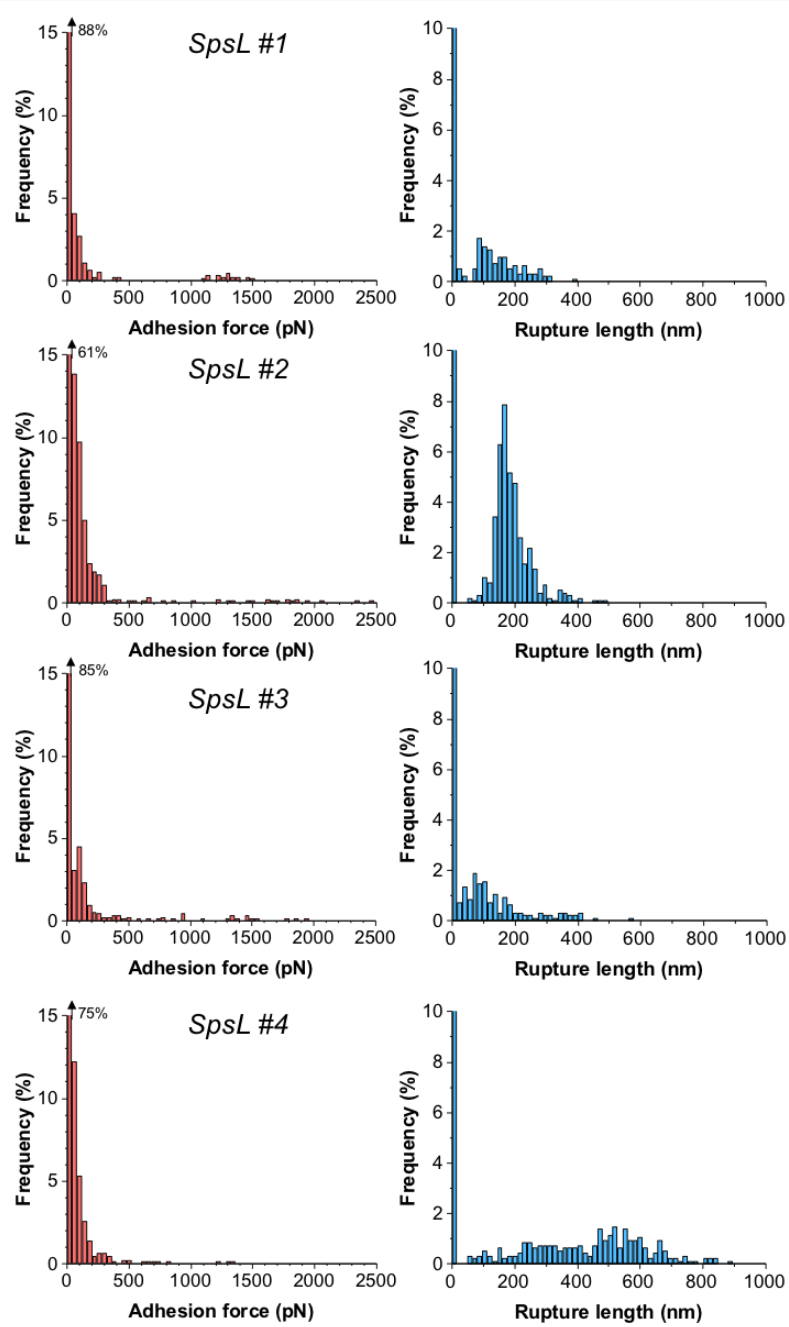

Figure 27: Binding strength of single SpsL-elastin bonds in living bacteria, obtained by SMFS. Maximum adhesion force (in red) and rupture length histograms (in blue) obtained by recording force-distance curves in PBS between four different S. pseudintermedius SpsL cells and AFM tips functionalized with elastin.

Table 3: Probability of adhesion (P_{adh}), adhesion force (F_{adh}) and rupture length (L_{rupt}) measured by SMFS between elastin-modified AFM tips and SpsL cells. The mean values are given with the corresponding standard deviation (mean ± s.d.).

	P_{adh} (%)	Low force regime < 500 pN							High force regime > 500 pN						
		F_{adh} (pN)				L_{rupt} (nm)			F_{adh} (pN)				L_{rupt} (nm)		
cell 1	16	141	±	99		150	±	116	1207	±	391		110	±	65
cell 2	30	144	±	95		296	±	193	1393	±	553		255	±	186
cell 3	6	73	±	16		101	±	69							
cell 4	6	62	±	15		94	±	55							
cell 5	12	104	±	83		231	±	192							
cell 6	15	148	±	111		271	±	157							
cell 7	12	113	±	82		153	±	73	1367	±	371		142	±	79
cell 8	65	113	±	44		383	±	101	874	±	261		480	±	312
cell 9	16	87	±	54		169	±	98	1178	±	204		178	±	85
cell 10	54	76	±	49		371	±	104	1176	±	377		182	±	91
cell 11	4	82	±	51		93	±	30							
cell 12	25	100	±	79		440	±	180	880	±	323		384	±	255
cell 13	39	114	±	73		182	±	46	1438	±	618		322	±	83

For both adhesins, though most the bonds rupture ~200 nm, we also noticed a bimodal distribution of the rupture lengths, which will be further discussed in section 5.2.

We also performed the same experiments on a mutant lacking both adhesins, *ΔspsDΔspsL*. Figure 28 presents the maximum adhesion force (left) and the rupture distance distribution (right), for such cells (n = 6 cells) interacting with elastin.

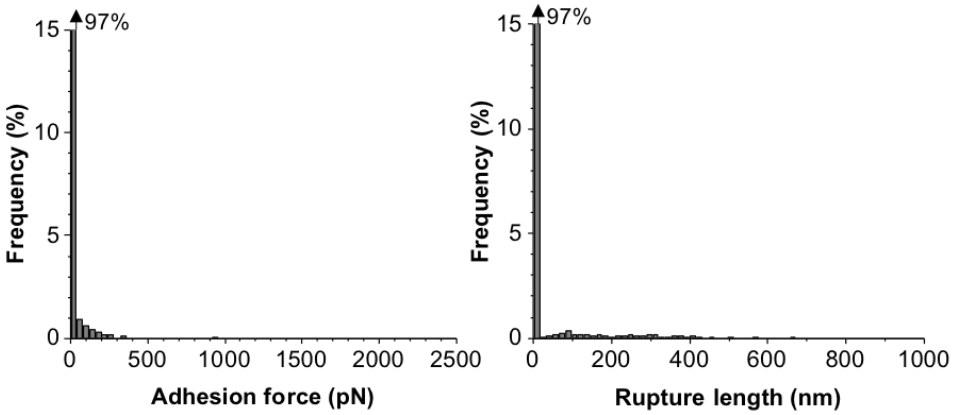

Figure 28: Binding strength of single ΔspsDΔspsL-elastin bonds in living bacteria, obtained by SMFS. Maximum adhesion force (left) and rupture length histograms (right) obtained by recording force-distance curves in PBS between six different S. pseudintermedius ΔspsDΔspsL cells and AFM tips functionalized with elastin merged forming one set of data.

Adhesive events were completely abrogated on these mutant cells suggesting that SpsD and SpsL adhesins were exclusively involved in the interaction with elastin. Thus, the adhesive

events observed in the previous experiments are attributed to the specific interaction of interest and not to unspecific ones.

During force volume experiment, adhesion maps are constructed pixel-by-pixel, by successively approaching and retracting the tip from the surface. Thus, along with the information (force and rupture length) extracted from the curves, we also obtained an adhesion map displaying the distribution of adhesive events (lighter pixels corresponding to higher forces). Adhesion maps obtained for both SpsD and SpsL cells showed significant differences in terms of adhesion probability, as already described above, and spatial distribution (Figure 29).

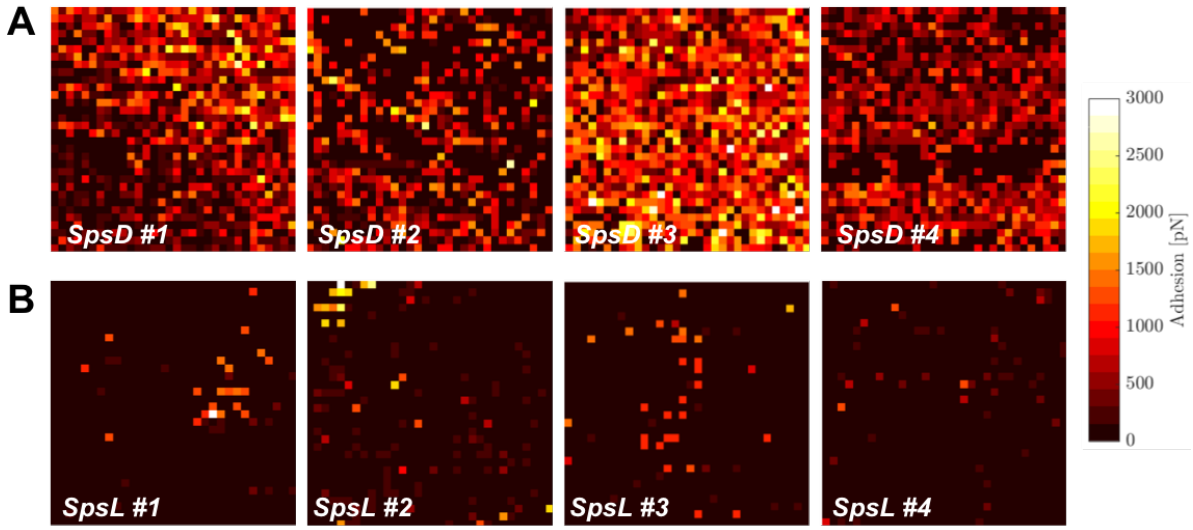

Figure 29: Adhesion maps recorded between elastin-tips and SpsD (A) and SpsL (B) cells. Maps were obtained by recording 32 by 32 force-distance curves on square areas of 0,25 µm² on top of the bacteria. Cells labelled here are the same as in Figure 25 and 27.

Adhesion maps revealed that, while SpsL cells present a random / heterogeneous distribution of adhesion events with elastin, SpsD cells display a homogeneous and dense distribution. Upon interaction with elastin, SpsD adhesins seem to be gathered together in nanodomains to form large clusters, at least covering a large part of the scanned area.

We can also estimate the density of the adhesins on the surface of the cell (Herman-Bausier et Dufrêne, 2016) considering the average binding probability, 68% for SpsD clusters and 23% for SpsL cells, and the size of adhesion maps, 1024 curves across 0.25 μm^2 areas. This leads to minimum surface densities of ~2785 and ~942 proteins per μm^2 respectively.

SpsD and SpsL showing both high and weak forces but to a different extent suggest that they may play different and / or complementary adhesive function. The results we obtained with elastin is, in that sense, reminiscent of the ones recently demonstrated by Viela *et al.* with SpsD and SpsL interacting with Fn. The authors suggested two distinct contributions for the two adhesins: while SpsL-Fn interactions are weak, facilitating the screening of host cells during

colonization, SpsD-Fn interactions are extremely strong allowing the firm attachment of bacteria to the host, even facing high shear stresses (Viela *et al*., 2020 b*)*.

5.3. An unexpected correlation between adhesion force and bond rupture

Previously we showed that SpsD- and SpsL-elastin bonds exhibited a kind of bimodal force distribution and were rupturing ~200 nm, though some bonds were breaking at much larger lengths. We wanted to investigate this behavior. Figure 30 presents a striking example of the bimodal distribution from a single SpsD and SpsL cells, both in terms of force and rupture length.

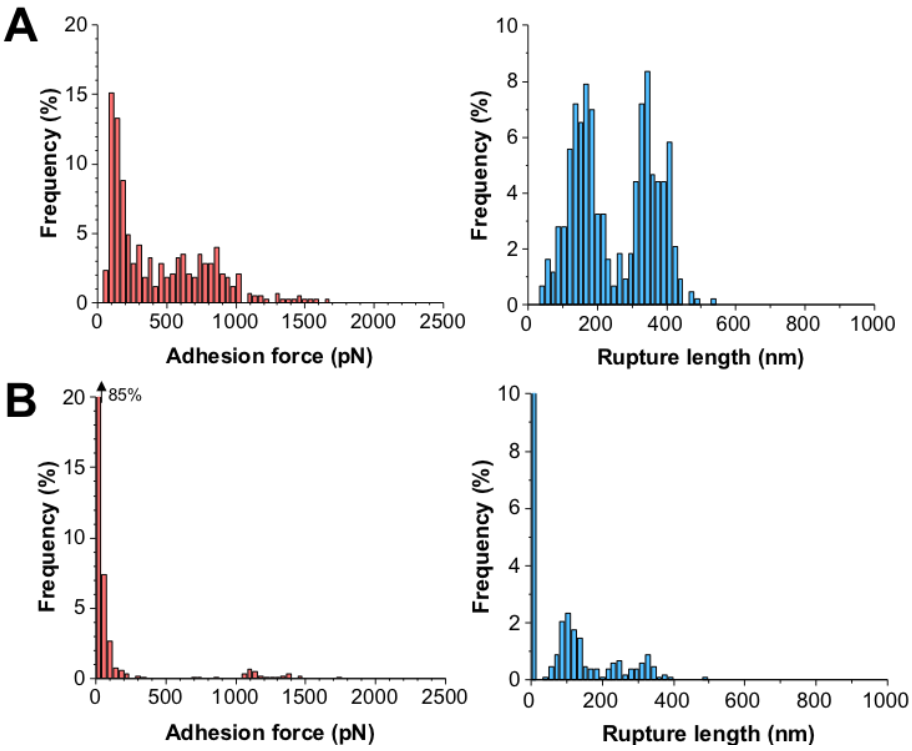

Figure 30: Binding strength between SpsD (A) and SpsL adhesins (B) and elastin obtained using SMFS. Maximum adhesion force (in red) and rupture length histograms (in blue) obtained by recording force-distance curves in PBS between S. pseudintermedius SpsD or SpsL cells and AFM tips functionalized with elastin.

Representative retraction force profiles are shown in Figure 31 for both the low (in red) and high force regime (in blue). One can easily notice that while low forces are associated with either short or long rupture lengths, high forces are mainly associated with short rupture lengths. Merging the results of three independent cells raise the same conclusion for both SpsD and SpsL cells: long rupture lengths were mainly associated with low forces (< 500 pN), most forces in the nN range breaking at shorter rupture length ~200 nm.

On average, strong forces ruptured at 226 ± 126 nm for SpsD (n = 798 data points), while weak ones were longer-ranged, 307 ± 162 nm, but with many values also in the 400-600 nm range

(n = 1254). Similarly, for SpsL cells strong forces ruptured at 189 ± 123 nm (n = 202) and weak ones at 294 ± 160 nm (n = 927).

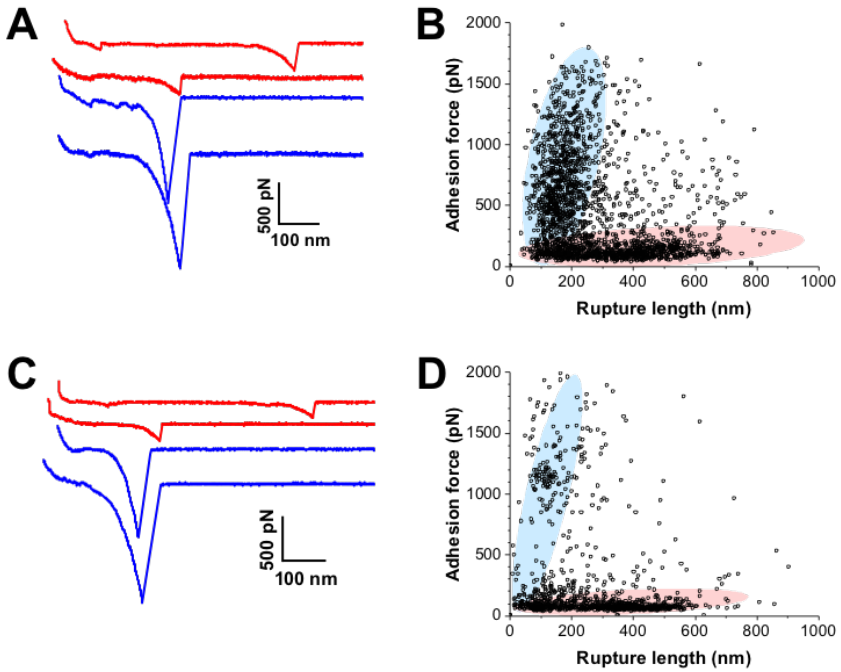

Figure 31: Representative retraction force profiles (left) of SpsD (A) or SpsL cells (C) and elastin and plots of adhesion forces versus rupture lengths (right) for three independent SpsD (B) or SpsL cells (D) (n = 2,052 and n = 1,129 data points for SpsD and SpsL, respectively). Results were obtained by recording force-distance curves in PBS between S. pseudintermedius SpsD cells (A, B) or SpsL cells (C, D) and AFM tips functionalized with elastin. Low force regime (red), high force regime (blue).

Assuming that the processed mature SpsD and SpsL adhesins comprise 1,031 and 930 residues respectively, that their folded length is about 20 nm and that each amino acid contributes 0.36 nm to the contour length of the polypeptide chain, the fully extended proteins should be ~350 nm and ~315 nm long respectively. This suggests that the adhesins largely extend and unfold in the long-range, low force regime, while they only extend (unfold) moderately in the short-range, high force regime. This intriguing behavior leads us to believe that Sps proteins interact with elastin via two interaction mechanisms, likely involving two distinct binding sites. As elastin is firmly attached to the tip via a multi-site chemistry, we expect it to contribute moderately to the observed elongations. However, the molecules might be orientated in different ways, and they are known to contain stretchable regions which might therefore contribute, to some extent, to the observed molecular extensions.

5.4 Force activates Sps-elastin interaction

It has been recently shown that the binding strength of staphylococcal adhesins can be dramatically enhanced by physical force (Herman-Bausier *et al., 2018)*. To investigate if such mechanically-activated mechanism was involved in the Sps- elastin interactions, we also performed loading rate (LR) experiments on our systems. The protocol is the same than in SMFS, but we varied the rate at which force is applied (0,5; 1,0; 3,0; 5,0; 10 µm/s) while

recording adhesion maps at those different rates always on the same area of the cell surface. An example of such experiment on a single SpsD cell is shown in Figure 32. Increasing the speed of retraction lead to a simultaneous increase in proportion of high forces and depletion of low forces.

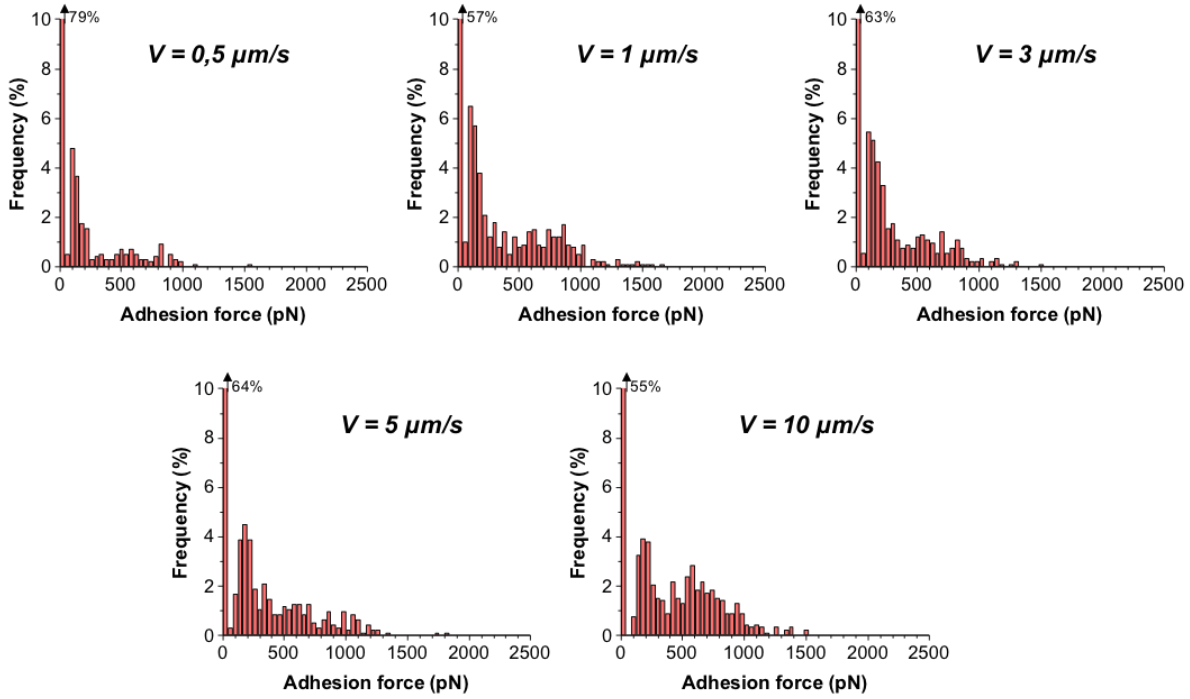

Figure 32: Adhesion force histograms at different rates. Adhesion forces were measured at various loading rates (LRs) between SpsD cell and elastin-tips on the same area.

The effective LR can be estimated for each FD curve from the force vs time curves (see Figure 21, section 4.3). Consequently, each adhesive event in the above histograms can be "translated" in a (force; LR) couple, usually presented in a dynamic force spectrum (DFS) plot (Figure 33).

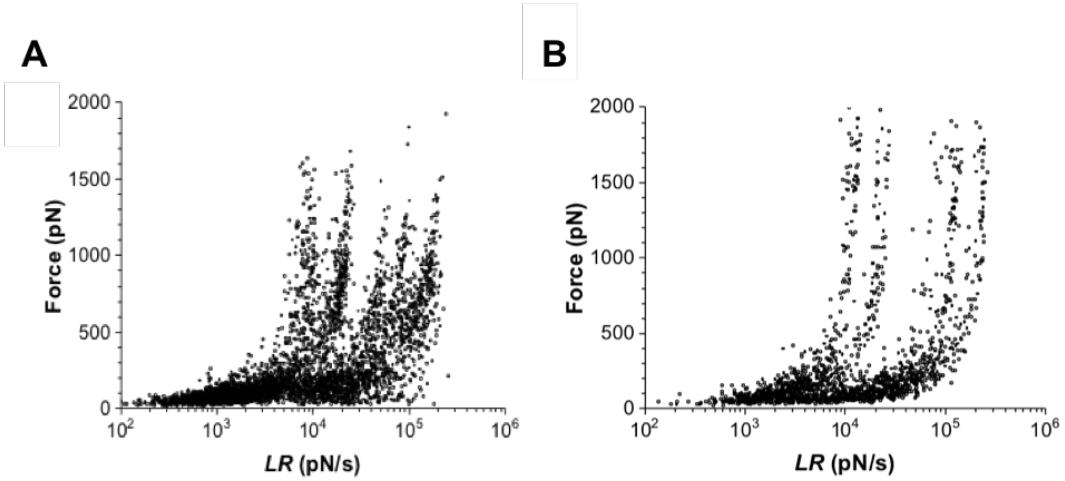

Figure 33: Dynamic force spectroscopy plot obtained by recording force-distance curves in PBS between elastin-tips and (A) SpsD cell (n = 4424 data points from the five maps) and (B) SpsL cell (n = 1788 data points from four independent SpsL cells).

The DFS plot for SpsD cells shows a cloudy distribution of forces as function of LR (Figure 33A). However, one can see that while increasing the LR, weak forces tend to decrease in proportion

whereas high forces tend to be populated, as previously shown in the force histograms at different speed. Concerning SpsL cells, results present the same tendency, a simultaneous increase of high forces and depletion of low forces when increasing the loading rate, as observed on the DFS plot (Figure 33B).

To further quantify this behavior, we analyzed force distributions over discrete ranges of LRs (Figure 34 and 35). Table 4 and 5 present the mean forces in low and high force regimes for the different range of LR for SpsD and SpsL respectively.

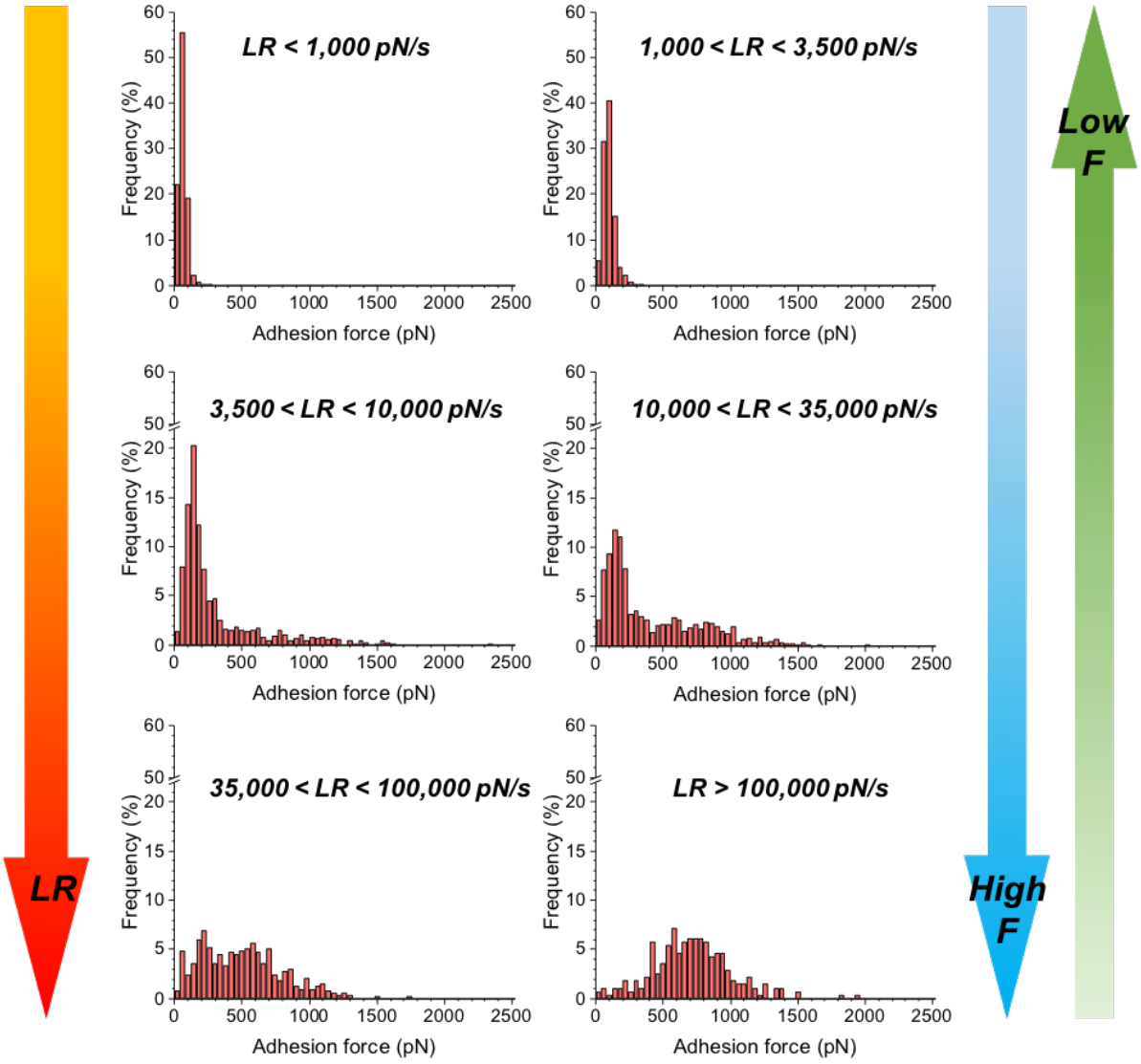

Figure 34: SpsD binds elastin through a force-dependent mechanism. *Adhesion force distribution at low and high loading rates (LRs), highlighting the shift towards higher forces (F) with increasing stress.*

For both SpsD and SpsL, the lowest LR (< 10,000 pN/s) showed mostly weak forces while the highest LR (> 100,000 pN/s) featured much higher forces. At intermediate LRs, weak and strong forces coexisted in various proportions. Therefore, the probability of forming strong bonds increases with the LR, implying that the Sps-elastin interaction strengthens with the applied force.

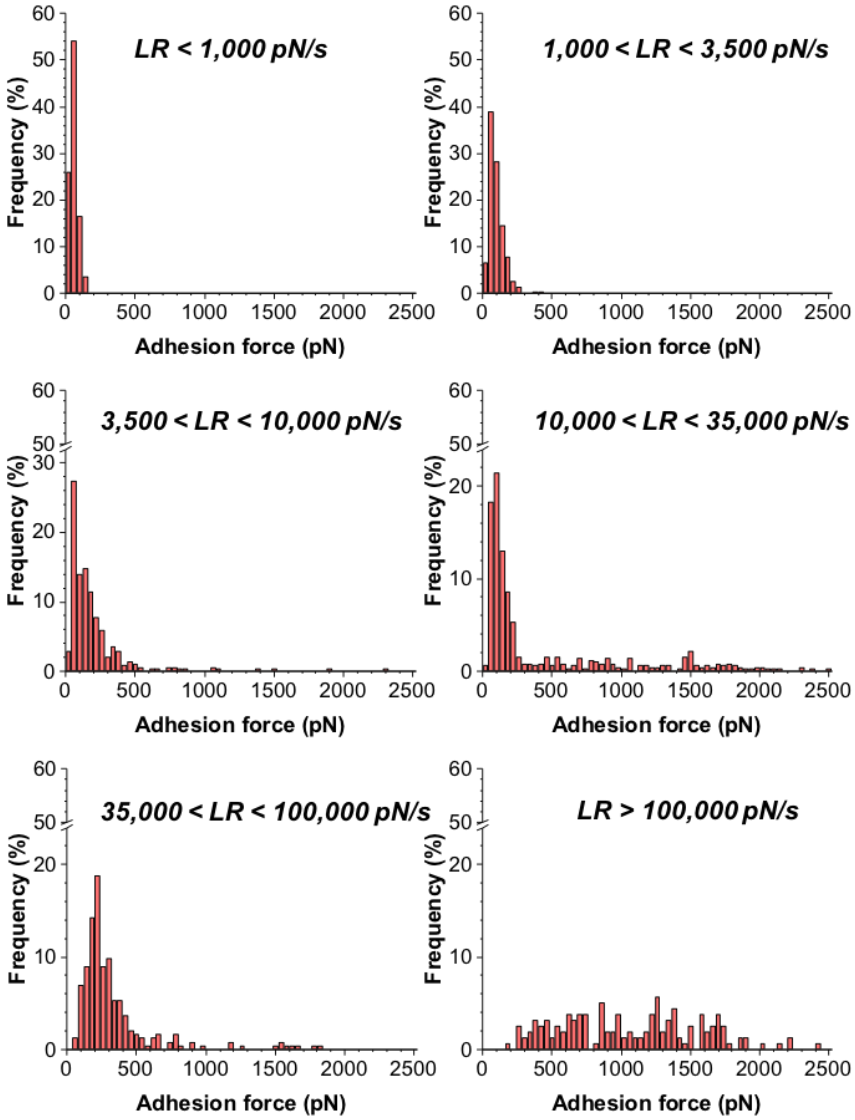

Figure 35: SpsL binds elastin through a force-dependent mechanism. Adhesion force distribution at low and high loading rates (LRs), highlighting the shift towards higher forces (F) with increasing stress.

Consequently, both SpsD- and SpsL-elastin interactions are mechanically activated. Nonetheless, considering the much lower adhesion probability of SpsL to elastin, it is likely that the two adhesins are involved in different adhesion strategies.

Table 4: Mean adhesion forces between SpsD cells and elastin at different LRs (mean ± s.d. (adhesion probability in %)).

	Low force regime (pN)	High force regime (pN)
LR < 1,000 pN/s	62 ± 29 (100 %)	
1,000 < LR < 3,500 pN/s	97 ± 45 (100 %)	
3,500 < LR < 10,000 pN/s	178 ± 98 (81 %)	921 ± 426 (19 %)
10,000 < LR < 35,000 pN/s	190 ± 112 (67 %)	880 ± 462 (33 %)
35,000 < LR < 100,000 pN/s	266 ± 130 (52 %)	754 ± 210 (48%)
LR > 100,000 pN/s	326 ± 136 (21 %)	815 ± 239 (79 %)

Table 5: Mean adhesion forces between SpsL cells and elastin at different LRs (mean ± s.d. (adhesion probability in %)).

	Low force regime (pN)	High force regime (pN)
LR < 1,000 pN/s	59 ± 28 (100 %)	
1,000 < LR < 3,500 pN/s	98 ± 53 (100 %)	
3,500 < LR < 10,000 pN/s	152 ± 101 (92 %)	943 ± 491 (8 %)
10,000 < LR < 35,000 pN/s	138 ± 89 (74 %)	1263 ± 496 (26 %)
35,000 < LR < 100,000 pN/s	237 ± 92 (85 %)	976 ± 496 (15%)
LR > 100,000 pN/s	375 ± 86 (16 %)	1235 ± 483 (84 %)

Such mechanically activated behavior could be due to conformational changes in the molecular complex formed by Sps and elastin. We thus looked at the spring constant of the molecular complex (K_m) (Figure 36) associated with the low and high force regimes, using the slope of the linear portion of the force vs tip position curves (see section 4.3).

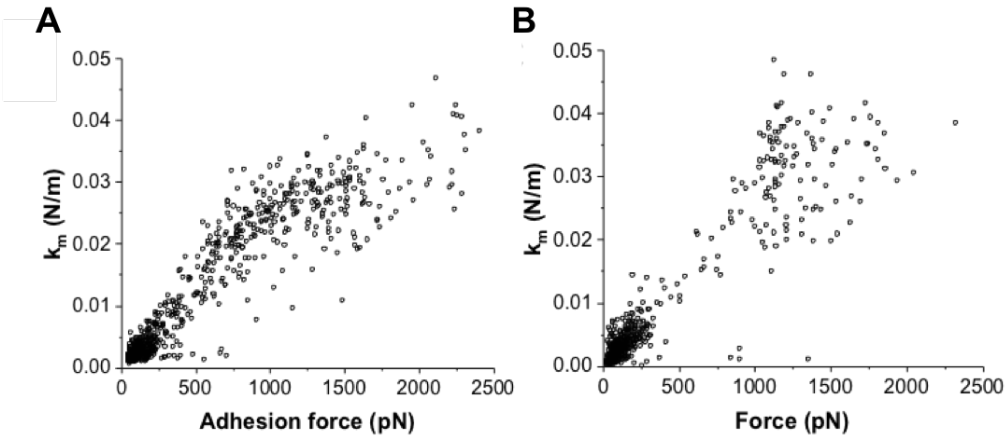

Figure 36: Scatter plot of the SpsD (A) and SpsL (B) -elastin molecular complex Km vs adhesion forces showing the switch to higher stiffness at high forces (n = 797 data points from three independent cells, n = 873 data points from three independent cells respectively).

We found for both Sps that the molecular stiffness increased linearly with the force, from 0.004 ± 0.003 N/m (n = 476 data points from 3 cells) to 0.024 ± 0.007 (n = 321), for SpsD (Figure 36A) and from 0.002. ± 0. 002 N/m (n = 737 data points from 3 cells) to 0.029 ± 0.009 (n = 136) for SpsL (Figure 36B), in the low and high force regimes. Hence, the increase in binding strength correlates with an increase in the stiffness of the molecular complex. Together with the difference in rupture lengths, this supports the view that weak and strong interactions are associated with different conformational states of the complex, a soft extended state and a stiff folded state.

5.5 A two binding site mechanism, involving a DLL

Our first striking results lie in the "bimodal" distributions of both adhesion force and rupture length for SpsD and SpsL adhesins interacting with elastin. SMFS experiments revealed (i) weak adhesion forces (low regime) around 200 pN for SpsD and 100 pN for SpsL associated with large rupture lengths of 300 nm respectively and (ii) stronger adhesion forces (high regime) around 1000 pN for SpsD and SpsL breaking at shorter length, 200 nm. Despite such similar behavior, SpsL cells were much less adhesive than SpsD cells, the probability of adhesion dropping from 68% to 23%, implying that SpsL and SpsD may play a different/complementary adhesive function in *S. pseudintermedius*. Recently, AFM experiments suggested two distinct contributions for the two adhesins while interacting with Fn: while SpsL-Fn interactions are weak, facilitating the screening of host cells during colonization, SpsD-Fn interactions are extremely strong allowing the firm attachment of bacteria to the host, even facing high shear stresses (Viela *et al*., 2020 b*)*. This complementarity might be also occurring when the pathogen interacts with elastin.

Furthermore, the ~1 nN forces (nearly equivalent to the strength of a covalent bond) exceeds by far the typical forces involved in protein-ligand interactions (~hundreds of pN). Thus, this ultrastrong interaction is in the same high magnitude of forces observed in the *S. epidermidis* SdrG-Fg interaction (~2 nN) (Herman *et al.,* 2014), (Milles *et al.,* 2018), known to follow a DLL mechanism which involves dynamic conformational changes of the adhesin resulting in a greatly stabilized adhesin-ligand complex (Figure 37).

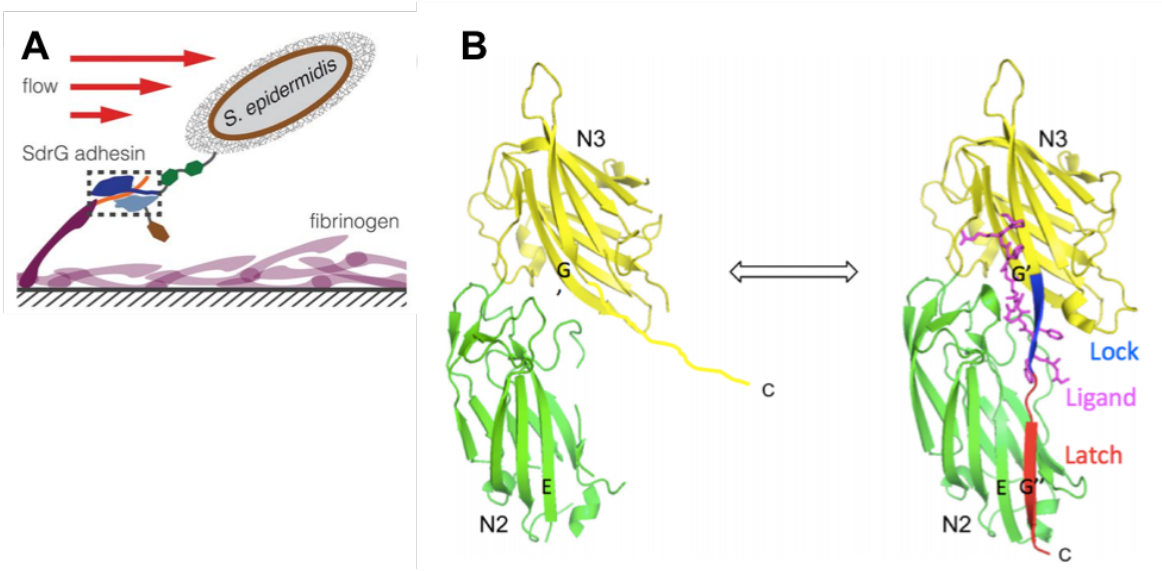

Figure 37: SdrG-Fg Binding by the Dock-Lock-Latch (DLL) Mechanism. (A) SdrG function, attached to the N-terminal peptide of the fibrinogen (purple) β chain (orange) adsorbed on a surface. This interaction prevents detachment of the bacterium by hydrodynamic force (Milles et al, 2018). (B) X-ray crystal structure of the apo form of the MSCRAMM SdrG with an open trench between subdomains N2 and N3. Upon binding of the Fg β-chain peptide the disordered C terminal extension of N3, which is not part of the apo form crystal structure, locks the ligand in place (blue) and forms the latch (red). Important β-strands are indicated (G, E) (Foster, 2019).

In details, Ponnuraj *et al*. solved in 2003, the structure of the ligand-binding domain of SdrG in complex with a synthetic peptide analogous to the binding site in its ligand, Fg. Analysis of the structure revealed that the SdrG protein has an open conformation that allows access of the ligand to a binding cleft. Following binding of the ligand, a structural rearrangement is induced at the C-terminus of the protein such that access to and from the binding cleft is blocked, and the 'docked' peptide is 'locked' in place. To stabilize the structure, the rearranged C-terminal β-sheet inserts between two β-sheets in an adjacent domain, 'latching' the protein-ligand complex together.

Previous studies revealed that molecular interactions following a DLL mechanism (such as SdrG-Fg, ClfA-Fg, ClfB-loricrin) are eventually mechanically-activated, *i.e.* their strength increase with external stress, such as those faced in physiological conditions (shear stress in bloodstream, contacts …) (Herman *et al.,* 2014), (Milles *et al.,* 2018).

Our loading rate experiments revealed that Sps-elastin interactions strengthen with the applied force: weak binding dominates at low stress, whereas strong binding is favored at high stress (Figure 38). This demonstrates that *S. pseudintermedius* adhesion, mediated by SpsD and SpsL, is also modulated in response to mechanical stress, which confirms the initial hypothesis of Pietrocola *et al.* stating that SpsD-elastin interaction follow a DLL mechanism (Pietrocola *et al*., 2013). SpsL appear to follow a similar mechanism though its much lower adhesion probability prevents us from undoubtedly concluding on the mechanism involved.

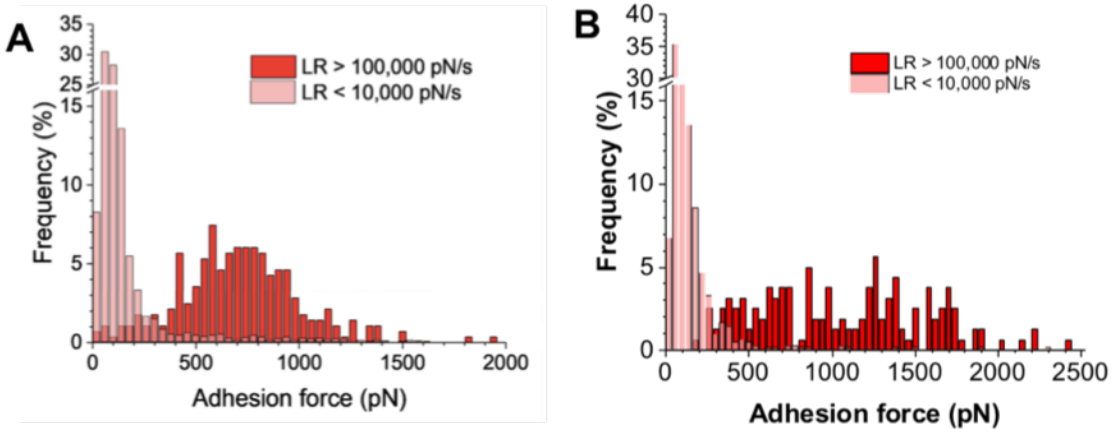

Figure 38: Adhesion force distribution at low and high loading rates (LRs) for SpsD cells (A) and SpsL cells (B), highlighting the shift towards higher forces with increasing stress.

Finally, we also demonstrated, especially for SpsD, that the transition from weak to strong forces correlates with an increase in molecular stiffness but also with a decrease in molecular extension, as mentioned above. Indeed, strong forces (1048 ± 204 pN) are short-ranged (226 ± 126 nm) and associated with high stiffness (0.024 ± 0.007), whereas weak ones (207 ± 57 pN) are of much longer-range (307 ± 162 nm) and softer (0.004 ± 0.003). This behavior has almost never been reported for a staphylococcal adhesion. We hypothesize that it results from two distinct binding mechanisms, regulated by mechanical force (Figure 39).

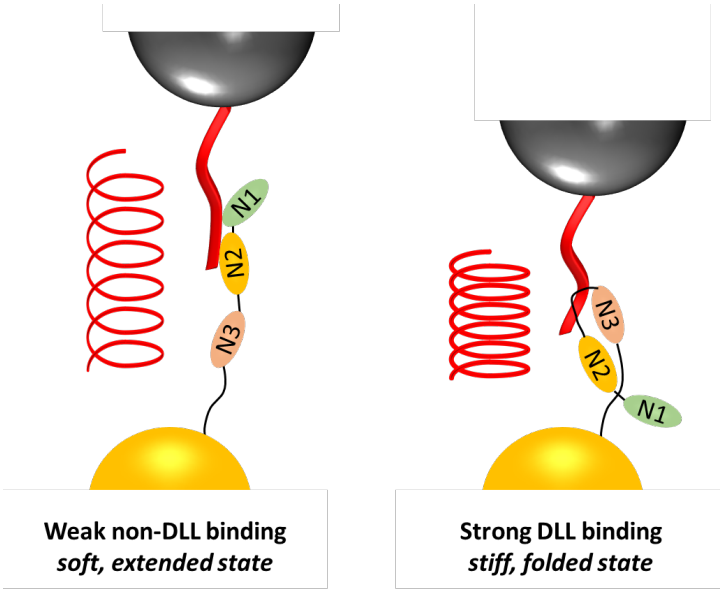

Figure 39: Proposed model for the force-dependent dual interaction of SpsD. The stiff, strong and short-ranged interaction arises from the DLL binding of elastin within the trench formed by the N2-N3 subdomains (right), whereas the soft, weak and extended interaction involves adhesion of elastin to a weak, non-DLL binding site of SpsD.

At low force, elastin would interact with a weak binding site of SpsD, leading to its extension and unfolding, while under high force, conformational changes of the SpsD N2-N3 subdomains would enable elastin to dock in the ligand binding trench and form strong DLL-like interactions as explained previously. Interestingly, Fg binding by ClfA involves two distinct sites, a DLL interaction between the trench of ClfA N2-N3 subdomains and the extreme C terminus of the γ-chain of Fg, and a second binding site located at the top of the N3 domain (Ganesh *et al.,* 2008).

6. Conclusions and perspectives

The specific adhesion of *S. pseudintermedius* to some ligands of the ECM is known to be mediated by SpsD and SpsL adhesins (Bannoehr *et al.*, 2012) (Pietrocola *et al.*, 2013). In this work, we have focused on the Sps-elastin interactions, since their molecular are poorly described even if their potential was previously highlighted (Pietrocola *et al.*, 2013). In order to understand the underlying mechanisms of these interactions, the forces involved in the binding of these adhesins to elastin and the dynamical behavior of such bonds have been investigated by Atomic Force Microscopy means.

Performing single cell and single molecule force spectroscopies, we investigated the mechanism involved in the Sps-elastin interactions and their dynamics. The results reported a bimodal distribution concerning the forces and the rupture length with an inverse correlation between both parameters. These so called low and high regimes suggest two different binding mechanisms. Concerning the high forces, it seems that the ultrastrong Sps-elastin interaction could result from a variation of a "dock, lock and latch" mechanism whereas the low forces result from a weaker binding mechanism. The rupture lengths being different depending on the regime, those mechanism would engage two distinct binding sites. Thus, our experiments suggest that, unlike the SdrG-Fg interaction (Herman *et al.,* 2014), Sps proteins interact with elastin via two distinct binding mechanisms, the adhesive function which is regulated by mechanical tension, following a variant of the DLL mechanism.

However, several experiments could be performed to further investigate the Sps-elastin interaction and confirm the suggested mechanism.

- Improving our SCFS experiments and interpretation

During the SCFS experiments we encountered difficulties in probing the interactions of interest probably due to the tendency of elastin to aggregate. Hence, some extra experiments are required to improve and further confirm our results on whole living cell. In order to optimize the results obtained from these experiments, we suggest some modifications of the protocol currently used to find a suitable way to perform SCFS on this interaction. The same experiments could be executed with a decreased amount of elastin grafted on the surface in order to avoid the aggregation, for instance by decreasing the amount of COOH to 1 % instead of 10 % during surface functionalization and/ or decreasing protein concentration. We could also modify experimental parameters such as pH and temperature trying though to stay under closely-related physiological conditions.

- Determining the nature of SpsD-elastin bond

The obtained results are similar to those observed in the ClfA-fg interaction. Indeed, the bond between ClfA and immobilized Fg is weak (~0.1 nN) at low tensile force but is dramatically enhanced (~1.5 nN) by mechanical tension (Herman-Bausier *et al.*, 2018). This behavior suggests the involvement of phenomenon called "catch bound", a specific bond that is reinforced by mechanical stress. Conversely to "slip bonds", where the strongest adhesion under flow is expected to occur at the lowest shear stress where force is the weakest, "catch bound" induces a mechanical resistance to the shear stress created, for example, by flow from the heart pumping blood, saliva, tear secretion or eyelid blinking. One compelling explanation for catch bonds is that force-induced structural alterations in the receptor protein are allosterically linked to a high-affinity conformation of its ligand-binding pocket (Figure 40) (Sokurenko *et al.*, 2008). At low force the bonds are weak and relatively short lived; with force increase, the bond's strength (i.e., lifetime) would increase to a certain level, after which a further increase in force would eventually break the bond.

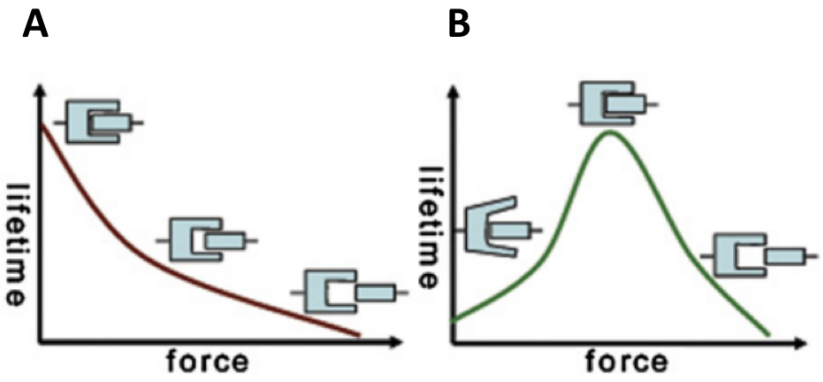

Figure 40: Dependence of the lifetime of receptor-ligand interactions on the force level in slip bonds (A) and in catch bonds (B) (Sokurenko et al.*, 2008).*

The presence of such interactions could be highlighted by "Force clamp" experiment, as it was performed on the SpsD-Fg interaction (Mathelié-Guinlet *et al.*, submitted), in order to measure the force-dependent bond lifetime. In force clamp measurements, a constant force is applied to the bond and the time until it disrupts is measured. This measured lifetime at a certain clamping force will not be unique but will follow an exponential distribution with an average value. Applying different levels of force and determining the corresponding average lifetime will directly lead to lifetime vs force plots. Thus, this type of measurements is particularly useful to detect catch bonds, in which moderate forces counterintuitively increase the lifetime of the bond (Rico *et al.,* 2011).

- Extending our findings to canine elastin

Up to now, we performed the experiments on the human elastin. However, *S. pseudintermedius* affects mainly dogs even if some zoonosis cases have been reported. We recognize the limitation of using human elastin to assess the role of this protein in this bacterial

infection of dogs. However, it should be noted that there is a high level of similarity between human and canine elastin. Based on the sequences found on Uniprot (ELN canin J9NW15, ELN human P15502) we performed a sequence alignment. Thanks to the Clustal Omega program, we computed the percentage of identity and similarity. The canine protein presents 527 aa whereas the human one presents 786 (55% identity). The difference is due to some deletions in the canine sequence. Taking into account these deletions, the sequences present 82% identity and 93% similarity. Knowing this high level of similarity, we could expect similar results for both human and canine elastin. However, Pickering *et al.* demonstrated, in 2019, that the SpsL adhesin has the ability to preferentially bind to canine Fg compared to other mammals Fg featuring a host-specific Fg-binding interaction. In their *in vitro* binding tests, results for canine and human Fg were similar but the SMFS results highlighted an important difference concerning the affinities and adhesion probabilities between both (Pickering *et al.,* 2019). Bannoehr *et al.* already suggested, in 2011, this host-specificity different for SpsD and SpsL. It seems thus interesting to perform AFM experiments on the Sps-canine elastin interaction in order to validate the suggested mechanism involved in the Sps-human elastin interaction (Bannoehr *et al*., 2011).

- Envisioning antibacterial therapies

As previously mentioned, unravelling the adhesion mechanisms of *S. pseudintermedius* could help in the design of novel anti-adhesion strategies. AFM is proving to be an important tool in this quest for new anti-adhesion strategies since it allows to reveal the mechanism involved in the interactions between pathogens and their substrate. It also makes it possible to test the effect of blocking agents, chosen based on the revealed mechanism, on the concerned interaction. Indeed, several studies show the potential suitability of AFM for the study of antiadhesive properties of small inhibitors targeting adhesins or pili. For instance, Viela *et al.* investigated the mechanostability of fibrinogen bridge between Staphylococcal surface protein ClfA and an endothelial cell Integrin in attendance of several blocking agents. Their results corroborate the finding of a potential antiadhesion drug against this interaction (Viela *et al.,* 2020 b). Similarly, Feuillie *et al.,* demonstrated the ability of a peptide derived from β-neurexin to block SdrC-dependent cell-surface attachment, cell-cell adhesion, and biofilm formation thanks to the AFM (Feuillie *et al., 2017)*. Thus, AFM might become an important tool to design these antiadhesion compounds to block cell adhesion (Viela *et al.,* 2020 a).

7. References

Albrecht, T. R., Grütter, P., Horne, D., Rugar, D., Jan. 1991. Frequency modulation detection using high- Q cantilevers for enhanced force microscope sensitivity. Journal of Applied Physics 69 (2), 668–673. http://doi.org/10.1063/1.347347

Almine, J.F., Bax, D.V., Mithieux, S.M., Nivison-Smith, L., Rnjak, J., Waterhouse, A., Wise, S.G., Weiss, A.S., 2010. Elastin-based materials. Chem Soc Rev 39, 3371–3379. https://doi.org/10.1039/b919452p

Bajwa, J., 2016. Canine superficial pyoderma and therapeutic considerations. Can Vet J 57, 204–206.

Baldock, C., Oberhauser, A. F., Ma, L., Lammie, D., Siegler, V., Mithieux, S. M., Tu, Y., Chow, J. Y. H., Suleman, F., Malfois, M., Rogers, S., Guo, L., Irving, T. C., Wess, T. J., Weiss, A. S., 2011. Shape of Tropoelastin, the Highly Extensible Protein That Controls Human Tissue Elasticity. Proc. Natl. Acad. Sci., 108 (11), 4322–4327. https://doi.org/10.1073/pnas.1014280108.

Bannoehr, J., Ben Zakour, N.L., Reglinski, M., Inglis, N.F., Prabhakaran, S., Fossum, E., Smith, D.G., Wilson, G.J., Cartwright, R.A., Haas, J., Hook, M., van den Broek, A.H.M., Thoday, K.L., Fitzgerald, J.R., 2011. Genomic and Surface Proteomic Analysis of the Canine Pathogen Staphylococcus pseudintermedius Reveals Proteins That Mediate Adherence to the Extracellular Matrix ▿. Infect Immun 79, 3074–3086. https://doi.org/10.1128/IAI.00137-11

Bannoehr, J., Guardabassi, L., 2012. Staphylococcus pseudintermedius in the dog: taxonomy, diagnostics, ecology, epidemiology and pathogenicity. Vet. Dermatol. 23, 253–266, e51-52. https://doi.org/10.1111/j.1365-3164.2012.01046.x

Beaussart, A., El-Kirat-Chatel, S., Herman, P., Alsteens, D., Mahillon, J., Hols, P., Dufrêne, Y.F., 2013. Single-cell force spectroscopy of probiotic bacteria. Biophys. J. 104, 1886–1892. https://doi.org/10.1016/j.bpj.2013.03.046

Binnig, G., Rohrer, H., Gerber, C., Weibel, E., 1982. Surface Studies by Scanning Tunneling Microscopy. Phys. Rev. Lett. 49, 5.

Binnig, G., Quate, C.F., Gerber, C., 1986. Atomic Force Microscope. Phys. Rev. Lett. 56, 5.

Casagrande Proietti, P., Stefanetti, V., Hyatt, D.R., Marenzoni, M.L., Capomaccio, S., Coletti, M., Bietta, A., Franciosini, M.P., Passamonti, F., 2015. Phenotypic and genotypic characterization of canine pyoderma isolates of Staphylococcus pseudintermedius for biofilm formation. J Vet Med Sci 77, 945–951. https://doi.org/10.1292/jvms.15-0043

Chambeaud, F., 2012. Les Staphylocoques en pathologie cutanée chez le chien: Connaissances actuelles.

Costerton, J.W., 1999. Bacterial Biofilms: A Common Cause of Persistent Infections. Science 284, 1318–1322. https://doi.org/10.1126/science.284.5418.1318

Daamen, W.F., Veerkamp, J.H., Hest, J.C.M. van, Kuppevelt, T.H. van, 2006. Elastin as a biomaterial for tissue engineering. Biomaterials 28, 4378–4398. https://doi.org/10.1016/j.biomaterials.2007.06.025

de Vos, W.M., 2015. Microbial biofilms and the human intestinal microbiome. NPJ Biofilms Microbiomes 1, 15005. https://doi.org/10.1038/npjbiofilms.2015.5

Donlan, R.M., 2002. Biofilms: microbial life on surfaces. Emerging Infect. Dis. 8, 881–890. https://doi.org/10.3201/eid0809.020063

Dufrêne, Y.F., 2008. Atomic force microscopy and chemical force microscopy of microbial cells. Nature Protocols 3, 1132–1138. https://doi.org/10.1038/nprot.2008.101

Dufrêne, Y.F., Ando, T., Garcia, R., Alsteens, D., Martinez-Martin, D., Engel, A., Gerber, C., Müller, D.J., 2017. Imaging modes of atomic force microscopy for application in molecular and cell biology. Nat Nanotechnol 12, 295–307. https://doi.org/10.1038/nnano.2017.45

Dufrêne, Y.F., Martínez-Martín, D., Medalsy, I., Alsteens, D., Müller, D.J., 2013. Multiparametric imaging of biological systems by force-distance curve–based AFM. Nature Methods 10, 847–854. https://doi.org/10.1038/nmeth.2602

Dufrêne, Y. F., Jun. 2015. Sticky microbes: forces in microbial cell adhesion. Trends in Micro- biology 23 (6), 376–382. http://linkinghub.elsevier.com/retrieve/pii/S0966842X15000256

Ebner, A., Hinterdorfer, P., Gruber, H. J., Oct. 2007. Comparison of different aminofunction- alization strategies for attachment of single antibodies to AFM cantilevers. Ultramicroscopy 107 (10-11), 922–927. http://linkinghub.elsevier.com/retrieve/pii/S0304399107001040

Feuillie, C., Formosa-Dague, C., Hays, L.M.C., Vervaeck, O., Derclaye, S., Brennan, M.P., Foster, T.J., Geoghegan, J.A., Dufrêne, Y.F., 2017. Molecular interactions and inhibition of the staphylococcal biofilm-forming protein SdrC. PNAS 114, 3738–3743. https://doi.org/10.1073/pnas.1616805114

Flemming, H.-C., Wingender, J., 2010. The biofilm matrix. Nat. Rev. Microbiol. 8, 623–633. https://doi.org/10.1038/nrmicro2415

Flemming, H.-C., Wingender, J., Szewzyk, U., Steinberg, P., Rice, S.A., Kjelleberg, S., 2016. Biofilms: an emergent form of bacterial life. Nat Rev Microbiol 14, 563–575. https://doi.org/10.1038/nrmicro.2016.94

Foster, T.J., 2019. The MSCRAMM Family of Cell-Wall-Anchored Surface Proteins of Gram-Positive Cocci. Trends in Microbiology 27, 927–941. https://doi.org/10.1016/j.tim.2019.06.007

Gaboriaud, F., Dufrêne, Y.F., 2007. Atomic force microscopy of microbial cells: Application to nanomechanical properties, surface forces and molecular recognition forces. Colloids and Surfaces B: Biointerfaces 54, 10–19. https://doi.org/10.1016/j.colsurfb.2006.09.014

Ganesh, V.K., Rivera, J.J., Smeds, E., Ko, Y.-P., Bowden, M.G., Wann, E.R., Gurusiddappa, S., Fitzgerald, J.R., Höök, M., 2008. A structural model of the Staphylococcus aureus ClfA-fibrinogen interaction opens new avenues for the design of anti-staphylococcal therapeutics. PLoS Pathog. 4, e1000226. https://doi.org/10.1371/journal.ppat.1000226

Garbacz, K., Żarnowska, S., Piechowicz, L., Haras, K., 2013. Pathogenicity potential of Staphylococcus pseudintermedius strains isolated from canine carriers and from dogs with infection signs. Virulence 4, 255–259. https://doi.org/10.4161/viru.23526

Garrett, T.R., Bhakoo, M., Zhang, Z., 2008. Bacterial adhesion and biofilms on surfaces. Progress in Natural Science 18, 1049–1056. https://doi.org/10.1016/j.pnsc.2008.04.001

Guillaume-Gentil, O., Potthoff, E., Ossola, D., Franz, C.M., Zambelli, T., Vorholt, J.A., 2014. Force-controlled manipulation of single cells: from AFM to FluidFM. Trends Biotechnol. 32, 381–388. https://doi.org/10.1016/j.tibtech.2014.04.008

Halan, B., Buehler, K., Schmid, A., 2012. Biofilms as living catalysts in continuous chemical syntheses. Trends Biotechnol. 30, 453–465. https://doi.org/10.1016/j.tibtech.2012.05.003

Hall-Stoodley, L., Stoodley, P., 2009. Evolving concepts in biofilm infections. Cell. Microbiol. 11, 1034–1043. https://doi.org/10.1111/j.1462-5822.2009.01323.x

Herman, P., El-Kirat-Chatel, S., Beaussart, A., Geoghegan, J.A., Foster, T.J., Dufrêne, Y.F., 2014. The binding force of the staphylococcal adhesin SdrG is remarkably strong. Mol. Microbiol. 93, 356–368. https://doi.org/10.1111/mmi.12663

Herman-Bausier, P., Dufrêne, Y.F., 2016. Atomic force microscopy reveals a dual collagen-binding activity for the staphylococcal surface protein SdrF. Molecular Microbiology 99, 611–621. https://doi.org/10.1111/mmi.13254

Herman-Bausier, P., Labate, C., Towell, A.M., Derclaye, S., Geoghegan, J.A., Dufrêne, Y.F., 2018. Staphylococcus aureus clumping factor A is a force-sensitive molecular switch that activates

bacterial adhesion. Proc. Natl. Acad. Sci. U.S.A. 115, 5564–5569. https://doi.org/10.1073/pnas.1718104115

Hinek, A., Rabinovitch, M., 1994. 67-kD elastin-binding protein is a protective “companion” of extracellular insoluble elastin and intracellular tropoelastin. J Cell Biol 126, 563–574.

Hinterdorfer, P., Dufrêne, Y.F., 2006. Detection and localization of single molecular recognition events using atomic force microscopy. Nature Methods 3, 347–355. https://doi.org/10.1038/nmeth871

Hnilica, K.A., Patterson, A.P. (Eds.), 2017. Chapter 3 - Bacterial Skin Diseases, in: Small Animal Dermatology (Fourth Edition). W.B. Saunders, 45–93. https://doi.org/10.1016/B978-0-323-37651-8.00003-1

Jamal, M., Ahmad, W., Andleeb, S., Jalil, F., Imran, M., Nawaz, M.A., Hussain, T., Ali, M., Rafiq, M., Kamil, M.A., 2018. Bacterial biofilm and associated infections. Journal of the Chinese Medical Association 81, 7–11. https://doi.org/10.1016/j.jcma.2017.07.012

Jørgensen, N.P., Zobek, N., Dreier, C., Haaber, J., Ingmer, H., Larsen, O.H., Meyer, R.L., 2016. Streptokinase Treatment Reverses Biofilm-Associated Antibiotic Resistance in Staphylococcus aureus. Microorganisms 4. https://doi.org/10.3390/microorganisms4030036

Kanta, J., 2016. Elastin in the Liver. Front Physiol 7. https://doi.org/10.3389/fphys.2016.00491

Keane, F. M., Clarke, A. W., Foster, T. J., Weiss, A. S., 2007. The N-Terminal A Domain of Staphylococcus Aureus Fibronectin-Binding Protein A Binds to Tropoelastin. Biochemistry, 46 (24), 7226–7232. https://doi.org/10.1021/bi700454x.

Kolter, R., Greenberg, E.P., 2006. Microbial sciences: the superficial life of microbes. Nature 441, 300–302. https://doi.org/10.1038/441300a

Kuo, C.-J., Ptak, C. P., Hsieh, C.-L., Akey, B. L., Chang, Y.-F., 2013. Elastin, a Novel Extracellular Matrix Protein Adhering to Mycobacterial Antigen 85 Complex. J. Biol. Chem., 288 (6), 3886–3896. https://doi.org/10.1074/jbc.M112.415679.

Lebeaux, D., Chauhan, A., Rendueles, O., Beloin, C., 2013. From in vitro to in vivo Models of Bacterial Biofilm-Related Infections. Pathogens 2, 288–356. https://doi.org/10.3390/pathogens2020288

Lebeaux, D., Ghigo, J.-M., 2012. Infections associées aux biofilms - Quelles perspectives thérapeutiques issues de la recherche fondamentale? Med Sci (Paris) 28, 727–739. https://doi.org/10.1051/medsci/2012288015

Lin, Y.-P., Lee, D.-W., McDonough, S. P., Nicholson, L. K., Sharma, Y., Chang, Y.-F., 2009. Repeated Domains of Leptospira Immunoglobulin-like Proteins Interact with Elastin and Tropoelastin. J. Biol. Chem., 284 (29), 19380–19391. https://doi.org/10.1074/jbc.M109.004531.

Little, S.V., Bryan, L.K., Hillhouse, A.E., Konganti, K., Lawhon, S.D., 2019. Whole-Genome Sequences of Staphylococcus pseudintermedius Isolates from Canine and Human Bacteremia Infections. Microbiol Resour Announc 8. https://doi.org/10.1128/MRA.00735-19

Macfarlane, S., Dillon, J., 2007. Microbial Biofilms in the Human Gastrointestinal Tract. Journal of applied microbiology. https://doi.org/10.1111/j.1365-2672.2007.03287.x

Mathelié-Guinlet, M., Viela, F., Viljoen, A., Dehullu, J., Dufrêne, Y.F., 2019. Single-molecule atomic force microscopy studies of microbial pathogens. Current Opinion in Biomedical Engineering, Molecular & CellularEngineering: single molecule technology. Neural Engineering: High Resolution Cell Imaging 12, 1–7. https://doi.org/10.1016/j.cobme.2019.08.001

Mecham, R.P., 2001. Overview of extracellular matrix. Curr Protoc Cell Biol Chapter 10, Unit 10.1. https://doi.org/10.1002/0471143030.cb1001s00

Milles, L.F., Schulten, K., Gaub, H.E., Bernardi, R.C., 2018. Molecular mechanism of extreme mechanostability in a pathogen adhesin. Science 359, 1527–1533. https://doi.org/10.1126/science.aar2094

Müller, D.J., Helenius, J., Alsteens, D., Dufrêne, Y.F., 2009. Force probing surfaces of living cells to molecular resolution. Nat. Chem. Biol. 5, 383–390. https://doi.org/10.1038/nchembio.181

Neu, T.R., Lawrence, J.R., 2015. Innovative techniques, sensors, and approaches for imaging biofilms at different scales. Trends in Microbiology 23, 233–242. https://doi.org/10.1016/j.tim.2014.12.010

O'Neill, E., Pozzi, C., Houston, P., Humphreys, H., Robinson, D.A., Loughman, A., Foster, T.J., O'Gara, J.P., 2008. A Novel Staphylococcus aureus Biofilm Phenotype Mediated by the Fibronectin-Binding Proteins, FnBPA and FnBPB. Journal of Bacteriology 190, 3835–3850. https://doi.org/10.1128/JB.00167-08

Patel, A., Fine, B., Sandig, M., Mequanint, K., 2006. Elastin biosynthesis: The missing link in tissue-engineered blood vessels. Cardiovasc Res 71, 40–49. https://doi.org/10.1016/j.cardiores.2006.02.021

Paul, N.C., Latronico, F., Moodley, A., Nielsen, S.S., Damborg, P., Guardabassi, L., 2013. In vitro adherence of Staphylococcus pseudintermedius to canine corneocytes is influenced by colonization status of corneocyte donors. Vet Res 44, 52. https://doi.org/10.1186/1297-9716-44-52

Park, P. W., Broekelmann, T. J., Mecham, B. R., Mecham, R. P., 1999. Characterization of the Elastin Binding Domain in the Cell-Surface 25-KDa Elastin-Binding Protein of Staphylococcus Aureus (EbpS). J. Biol. Chem., 274 (5), 2845–2850. https://doi.org/10.1074/jbc.274.5.2845.

Parks, W.C., Pierce, R.A., Lee, K.A., Mecham, R.P., 1993. Advance in molecular and cell biology, Vol. 6, edited by Kleinman, H.K., 133-182.

Perreten, V., Kadlec, K., Schwarz, S., Grönlund Andersson, U., Finn, M., Greko, C., Moodley, A., Kania, S.A., Frank, L.A., Bemis, D.A., Franco, A., Iurescia, M., Battisti, A., Duim, B., Wagenaar, J.A., van Duijkeren, E., Weese, J.S., Fitzgerald, J.R., Rossano, A., Guardabassi, L., 2010. Clonal spread of methicillin-resistant Staphylococcus pseudintermedius in Europe and North America: an international multicentre study. J. Antimicrob. Chemother. 65, 1145–1154. https://doi.org/10.1093/jac/dkq078

Pickering, A.C., Vitry, P., Prystopiuk, V., Garcia, B., Höök, M., Schoenebeck, J., Geoghegan, J.A., Dufrêne, Y.F., Fitzgerald, J.R., 2019. Host-specialized fibrinogen-binding by a bacterial surface protein promotes biofilm formation and innate immune evasion. PLoS Pathog 15. https://doi.org/10.1371/journal.ppat.1007816

Pietrocola, G., Geoghegan, J.A., Rindi, S., Di Poto, A., Missineo, A., Consalvi, V., Foster, T.J., Speziale, P., 2013. Molecular Characterization of the Multiple Interactions of SpsD, a Surface Protein from Staphylococcus pseudintermedius, with Host Extracellular Matrix Proteins. PLoS One 8. https://doi.org/10.1371/journal.pone.0066901

Pietrocola, G., Gianotti, V., Richards, A., Nobile, G., Geoghegan, J.A., Rindi, S., Monk, I.R., Bordt, A.S., Foster, T.J., Fitzgerald, J.R., Speziale, P., 2015. Fibronectin Binding Proteins SpsD and SpsL Both Support Invasion of Canine Epithelial Cells by Staphylococcus pseudintermedius. Infect. Immun. 83, 4093–4102. https://doi.org/10.1128/IAI.00542-15

Pires dos Santos, T., Damborg, P., Moodley, A., Guardabassi, L., 2016. Systematic Review on Global Epidemiology of Methicillin-Resistant Staphylococcus pseudintermedius: Inference of Population Structure from Multilocus Sequence Typing Data. Front Microbiol 7. https://doi.org/10.3389/fmicb.2016.01599

Podrazky, V., 1967. Reconstitution of Elastin. Nature 215, 1162–1163. https://doi.org/10.1038/2151162a0

Pompilio, A., De Nicola, S., Crocetta, V., Guarnieri, S., Savini, V., Carretto, E., Di Bonaventura, G., 2015. New insights in Staphylococcus pseudintermedius pathogenicity: antibiotic-resistant

biofilm formation by a human wound-associated strain. BMC Microbiol 15. https://doi.org/10.1186/s12866-015-0449-x

Ponnuraj, K., Bowden, M.G., Davis, S., Gurusiddappa, S., Moore, D., Choe, D., Xu, Y., Hook, M., Narayana, S.V.L., 2003. A “dock, lock, and latch” Structural Model for a Staphylococcal Adhesin Binding to Fibrinogen. Cell 115, 217–228. https://doi.org/10.1016/S0092-8674(03)00809-2

Radmacher, M., 2002. Measuring the elastic properties of living cells by the atomic force microscope. Methods Cell Biol. 68, 67–90. https://doi.org/10.1016/s0091-679x(02)68005-7

Reffuveille, F., Josse, J., Vallé, Q., Gangloff, C.M. and S.C., 2017. Staphylococcus aureus Biofilms and their Impact on the Medical Field. The Rise of Virulence and Antibiotic Resistance in Staphylococcus aureus. https://doi.org/10.5772/66380

Richards, A.C., O’Shea, M., Beard, P.M., Goncheva, M.I., Tuffs, S.W., Fitzgerald, J.R., Lengeling, A., 2018. Staphylococcus pseudintermedius Surface Protein L (SpsL) Is Required for Abscess Formation in a Murine Model of Cutaneous Infection. Infect. Immun. 86. https://doi.org/10.1128/IAI.00631-18

Rico, F., Zhang, X., Moy, V.T., 2019. Probing Cellular Adhesion at the Single-Molecule Level, edited by Dufrene, Y., Life at the Nanoscale: Atomic Force Microscopy of Live Cells. CRC Press.

Roche, F. M., Downer, R., Keane, F., Speziale, P., Park, P. W., Foster, T. J., 2004. The N-Terminal A Domain of Fibronectin-Binding Proteins A and B Promotes Adhesion of Staphylococcus Aureus to Elastin. J. Biol. Chem., 279 (37), 38433–38440. https://doi.org/10.1074/jbc.M402122200.

Rosenstein, R., Götz, F., 2013. What distinguishes highly pathogenic staphylococci from medium- and non-pathogenic? Curr. Top. Microbiol. Immunol. 358, 33–89. https://doi.org/10.1007/82_2012_286

Singh, A., Walker, M.A., Rousseau, J., Weese, J.S., 2013. Characterization of the biofilm forming ability of Staphylococcus pseudintermedius from dogs, in: BMC Veterinary Research. https://doi.org/10.1186/1746-6148-9-93

Smallman, R.E., Ngan, A.H.W., 2014. Chapter 5 - Characterization and Analysis, in: Smallman, R.E., Ngan, A.H.W. (Eds.), Modern Physical Metallurgy (Eighth Edition). Butterworth-Heinemann, Oxford, pp. 159–250. https://doi.org/10.1016/B978-0-08-098204-5.00005-5

Sokurenko, E., V, V., We, T., 2008. Catch-bond Mechanism of Force-Enhanced Adhesion: Counterintuitive, Elusive, but ... Widespread? Cell host & microbe. https://doi.org/10.1016/j.chom.2008.09.005

Tsang, K.Y., Cheung, M.C.H., Chan, D., Cheah, K.S.E., 2010. The developmental roles of the extracellular matrix: beyond structure to regulation. Cell Tissue Res. 339, 93–110. https://doi.org/10.1007/s00441-009-0893-8

van Duijkeren, E., Kamphuis, M., van der Mije, I.C., Laarhoven, L.M., Duim, B., Wagenaar, J.A., Houwers, D.J., 2011. Transmission of methicillin-resistant Staphylococcus pseudintermedius between infected dogs and cats and contact pets, humans and the environment in households and veterinary clinics. Veterinary Microbiology 150, 338–343. https://doi.org/10.1016/j.vetmic.2011.02.012

Van Hoovels, L., Vankeerberghen, A., Boel, A., Van Vaerenbergh, K., De Beenhouwer, H., 2006. First Case of Staphylococcus pseudintermedius Infection in a Human. J Clin Microbiol 44, 4609–4612. https://doi.org/10.1128/JCM.01308-06

Viela, F., Mathelié-Guinlet, M., Viljoen, A., Dufrêne, Y.F., 2020 a. What makes bacterial pathogens so sticky? Molecular Microbiology 113, 683–690. https://doi.org/10.1111/mmi.14448

Viela, F., Speziale, P., Pietrocola, G., Dufrêne, Y.F., 2020 b. Mechanostability of the Fibrinogen Bridge between Staphylococcal Surface Protein ClfA and Endothelial Cell Integrin αV β3. Nano Letters. https://doi.org/10.1021/acs.nanolett.9b03080

Viljoen, A., Mignolet, J., Viela, F., Mathelié-Guinlet, M., Dufrêne, Y.F., 2020. How microbes use force to control adhesion. Journal of Bacteriology. https://doi.org/10.1128/JB.00125-20

Vrhovski, B., Weiss, A.S., 1998. Biochemistry of tropoelastin. Eur. J. Biochem. 258, 1–18. https://doi.org/10.1046/j.1432-1327.1998.2580001.x

Weisenhorn, A.L., Hansma, P.K., Albrecht, T.R., Quate, C.F., 1989. Forces in atomic force microscopy in air and water. Applied Physics Letters 54, 2651–2653. https://doi.org/10.1063/1.101024

Westerlund, B., Korhonen, T.K., 1993. Bacterial proteins binding to the mammalian extracellular matrix. Molecular Microbiology 9, 687–694. https://doi.org/10.1111/j.1365-2958.1993.tb01729.x

Wladyka, B., Piejko, M., Bzowska, M., Pieta, P., Krzysik, M., Mazurek, Ł., Guevara-Lora, I., Bukowski, M., Sabat, A.J., Friedrich, A.W., Bonar, E., Międzobrodzki, J., Dubin, A., Mak, P., 2015. A peptide factor secreted by Staphylococcus pseudintermedius exhibits properties of both bacteriocins and virulence factors. Sci Rep 5. https://doi.org/10.1038/srep14569

Yeo, G.C., Keeley, F.W., Weiss, A.S., 2011. Coacervation of tropoelastin. Adv Colloid Interface Sci 167, 94–103. https://doi.org/10.1016/j.cis.2010.10.003

Yue, B., 2014. Biology of the Extracellular Matrix: An Overview. J Glaucoma S20–S23. https://doi.org/10.1097/IJG.0000000000000108

Nanomechanics of the molecular complexes between SpsD/SpsL staphylococcal adhesins and elastin

Constance Chantraine

Staphylococcus pseudintermedius is a commensal pathogen having the capacity to develop biofilms. Bacterial adhesion to the host extracellular matrix (mainly dogs but humans too) is known to be mediated by the SpsD and SpsL adhesins. Considering the emergence of zoonosis cases for *S. pseudintermedius* and the increasing occurrence of methicillin-resistant strains, it is now crucial to unravel the mechanisms by which the pathogen adheres to-, and in turn infect, its hosts. In this context, we studied the strength and dynamics of interaction between SpsD/SpsL and elastin, a key matrix protein critical to the elasticity and resilience of many vertebrate tissues. To this end, we used atomic force microscopy, which allows to quantify the mechanical strength of single receptor-ligand complexes. We observed a bimodal distribution of the forces and rupture lengths with an inverse correlation between both parameters. These so called low and high force regimes suggest two different binding mechanisms. We also found that both SpsD- and SpsL-elastin interactions are mechanically activated. Weak binding dominates at low stress, whereas strong binding is favored at high stress. We suggest that the ultrastrong Sps-elastin interaction could result from a variation of the “dock, lock and latch” mechanism whereas the low adhesion force results from a weaker binding mechanism. Our results offer promise for the design of novel anti-adhesion strategies thereby helping in the prevention of biofilm formation and infection.

UNIVERSITÉ CATHOLIQUE DE LOUVAIN
Faculté des bioingénieurs
Croix du Sud, 2 bte L7.05.01, 1348 Louvain-la-Neuve, Belgique | **www.uclouvain.be/agro**